

Diffusion versus recrystallization processes in Rb–Sr geochronology: Isotopic relics in eclogite facies rocks, Western Gneiss Region, Norway

Johannes Glodny ^{a,*}, Alexander Kühn ^{b,1}, Håkon Austrheim ^c

^a *GeoForschungsZentrum Potsdam, Telegrafenberg C2, 14473 Potsdam, Germany*

^b *Institut für Geowissenschaften, Johannes Gutenberg-Universität, Becherweg 21, 55099 Mainz, Germany*

^c *PGP and Department of Earth Sciences, Postboks 1047, University of Oslo, N-0316 Oslo, Norway*

Received 23 January 2007; accepted in revised form 29 October 2007; available online 4 November 2007

Abstract

Rb–Sr and U–Pb isotopic data for granulite facies rocks, forming textural relics with respect to eclogite facies metamorphism in the Western Gneiss Region (WGR) of Norway, highlight the importance of textures and mineral reaction kinetics for the interpretation of geochronological data. Studied rocks from Bårdsholmen, southern WGR, were subjected to granulite facies metamorphism at 955 ± 3 Ma (U–Pb, zircon). Later on, they experienced a subduction-related, kinetically stranded eclogitization ($T > 650$ °C at ~ 20 kbar) at 404 ± 2 Ma (Rb–Sr multiminerall internal isochron data), followed by exhumation through amphibolite facies conditions. Full conversion of granulite to eclogite was restricted to zones of fluid infiltration and deformation. Despite the fact that metamorphic temperatures vastly exceeded the commonly assumed ‘closure temperature’ for Rb–Sr in submillimeter-sized biotite for several Ma during eclogite facies overprint, Sr-isotopic signatures of relic biotite have not been fully reset. Large biotite crystals nearly record their Sveconorwegian (Grenvillian) crystallization age. Sr signatures of other granulite facies phases (feldspar, pyroxenes, amphibole) remained unchanged, with the exception of apatite. The results imply that isotopic signatures much closer correspond to the P , T conditions of formation recorded by a dated phase and its paragenesis, than to a temperature history. In texturally well-equilibrated high-grade rocks which experienced no mineral reactions and remained devoid of free fluids during exhumation, like granulites or eclogites, isotopic resetting during cooling is either kinetically locked, or restricted to sluggish intermineral diffusion which demonstrably does not lead to full isotopic homogenization. In texturally unequilibrated rocks, textural relics are likely to represent isotopic relics. It is shown that for both high-grade rocks and for rocks with textural disequilibria, geologically meaningful isotopic ages based on isochron methods can only be derived from sub-assemblages in isotopic equilibrium, which have to be defined by analysis of all rock-forming minerals. Conventional two-point ‘mica ages’ for such rocks are a priori geochronologically uninterpretable, and valid multiminerall isochron ages a priori do not record cooling but instead date recrystallization-inducing processes like fluid–rock interaction.

© 2007 Elsevier Ltd. All rights reserved.

1. INTRODUCTION

A persistent challenge in radiogenic isotope geochronology is to accurately link isotopic age data to specific pro-

cesses in a rock, like crystallization and recrystallization, fluid–rock interaction, metamorphic mineral reactions, deformation, and cooling. This step in the interpretation of isotopic data is critical if data are to be converted to geodynamic information on nature and velocity of orogenic processes at depth. Two fundamental factors have been identified capable of setting and modifying element distribution signatures as well as isotopic signatures of the widely

* Corresponding author. Fax: +49 331 2881370.

E-mail address: glodnyj@gfz-potsdam.de (J. Glodny).

¹ Gexco AS, Postboks 500, 8601 Mo i Rana, Norway.

used Rb–Sr, K–Ar, U–Pb and Sm–Nd systems in rocks and minerals, namely (a) recrystallization-inducing processes, like deformation and fluid–rock interaction with dissolution/reprecipitation, and (b) temperature-driven diffusion (see Villa, 2006 for review). The potential of temperature-driven diffusion to modify isotopic mineral signatures in rocks has been discussed for long. It has been used to develop elaborate concepts, essentially translating diffusivities of radiogenic nuclides within specific minerals into a narrow temperature range separating high-temperature nuclide mobility from low-temperature immobility, the so-called ‘blocking temperature’ or ‘closure temperature’ (e.g., Jäger, 1967; Dodson, 1973; Lovera et al., 1989). A system of different closure temperatures for different decay systems in a number of minerals has been established, which is often used to infer thermal histories of geologic units. Isotope diffusivities in this context have either been deduced from natural examples, i.e., from isotopic signatures in rocks with well-constrained thermal histories, or from experimental diffusion data. While extrapolation of experimental diffusion or other kinetic data to geological timescales and temperatures is fraught with difficulties (see Baxter and DePaolo, 2002; Villa, 2006), some of the early geological studies of isotopic closure were biased towards a search for temperature effects, and did not take adequately into account other factors than temperature influencing isotope signatures.

Geochronological studies involving independent textural information or observational data from microanalytical techniques, like electron microprobe analysis or cathodoluminescence imaging, generally reveal close linkage between isotopic signatures, texture, and mineral growth zoning (e.g., Vance et al., 2003, and references therein). Results are often in contrast with expectations solely based on thermochronological concepts. It has been perceived that in specific situations isotopic signatures persist through temperatures far above commonly considered ‘closure temperatures’, and that apparent closure temperatures of individual mineral grains in a rock may strongly depend on their textural position. Among the most prominent examples is the survival of Ar-isotopic microscale disequilibria in polygenetic white mica through metamorphic temperatures exceeding 600 °C (Giorgis et al., 2000; Di Vincenzo et al., 2001). The persistence of Rb–Sr biotite signatures in ultramafic rocks through eclogite facies metamorphism (Kühn et al., 2000) and the unaltered preservation of Rb–Sr phengite signatures set at >600 °C in eclogites (Glodny et al., 2003, 2005) can be explained by *modally controlled closed system behavior* (see discussion in Glodny et al., 2003). *Shielding* is another mechanism that can prevent isotopic systems from being reset even at extreme temperatures (Montel et al., 2000).

However, for many natural rocks it is difficult to distinguish whether diffusive isotope redistribution was potentially significant, or whether in fact the observed isotope signatures relate to recrystallization-inducing processes. Not much is actually known about the specific signatures which solely temperature-driven isotope transport and isotope redistribution leaves in a rocks’ mineral isotope systematics. This is surprising given the abundant

‘thermochronological’ interpretations of isotopic data. We designed the present study to isolate the effect of temperature on the Rb–Sr isotopic evolution of a natural rock system submitted to an eclogite-facies thermal overprint, and consequently to assess the validity of the closure temperature concept in absence of recrystallization. Granulite facies rocks exhibiting a kinetically stranded eclogitization with low overall reaction progress should allow to define temperature-related Sr isotope redistribution effects on the granulitic relic assemblage and to distinguish these effects from recrystallization-related Sr mobility.

This case study is based on rocks from the well described locality of Bårdsholmen, Dalsfjord area, Western Gneiss Region (WGR), Norway (Engvik et al., 2000). There a Sveconorwegian (Grenvillean) granulite facies complex shows a Caledonian eclogite facies overprint, visible both macroscopically and as reaction rims along grain boundaries and cracks (cf. Engvik et al., 2000). Phases belonging to the relic, granulite facies reactant assemblage can clearly be discerned from those of the eclogite facies product assemblage. Literature data suggest that here eclogite-facies metamorphic temperatures ($T > 650$ °C; Engvik and Andersen, 2000; Foreman et al., 2005) largely exceeded those commonly considered as ‘closure temperatures’ for Rb–Sr in biotite, apatite, and Na–K-feldspar.

We report Rb–Sr isotope systematics on the mineral scale of partially eclogitized mafic granulites. To constrain the metamorphic history in detail, we present new P , T estimates on the two metamorphic events, as well as U/Pb zircon and Rb/Sr multimineral isochron age data. The results show that textural relics translate into Sr-isotopic relics, even through prolonged episodes of high grade metamorphism. Exclusively temperature-induced Sr isotope redistribution in a rock does not lead to full intermineral isotopic re-equilibration, and is detectable from characteristic Sr isotopic disequilibrium distribution patterns.

2. GEOLOGICAL SETTING

2.1. The Western Gneiss Region

The Western Gneiss Region (WGR) in western Norway (Fig. 1) is the deepest exposed unit of the Scandinavian Caledonides. It is dominated by Paleo- to Mesoproterozoic gneisses, some with Grenvillean metamorphic overprint (at ~1000–950 Ma; Gaál and Gorbatshev, 1987; Skår and Pedersen, 2003). Metabasic rocks and metamorphosed upper crustal lithologies occur as well (Brynhi and Sturt, 1985; Bryhni, 1989). During the Caledonian continent–continent collision, the WGR formed part of the subducted leading edge of Baltica, and has been subjected to eclogite facies, HP to UHP conditions (Griffin and Brueckner, 1980; Cuthbert et al., 2000). Occurrences of microdiamonds and coesite in the NW part of the WGR testify to subduction of continental crust to depths exceeding ~100 km (Carswell et al., 2003b, and references therein). Available high-precision geochronology constrains eclogitization between 415–410 Ma (northwestern part of the WGR) and 405–400 Ma in the central-western part of the WGR (see review by Hacker, 2007). Eclogites occur in a tectonic window

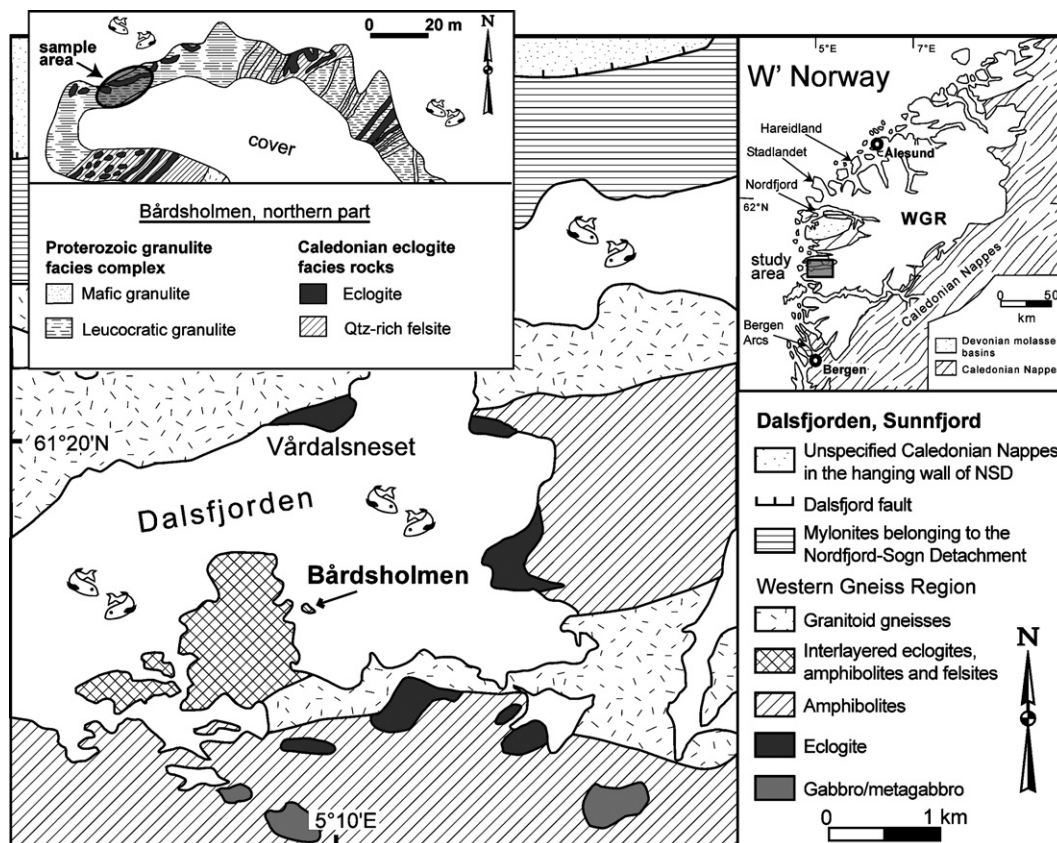


Fig. 1. Geological map of the Dalsfjord region, West Norway (redrawn after Engvik et al., 2000) showing the location of the island of Bårdsholmen; NSD, Nordfjord-Sogn Detachment. (Inset) Geological map of Bårdsholmen, showing the distribution of granulite-, eclogite- and amphibolite-facies equivalents of the mafic and leucocratic lithologies (after Engvik et al., 2000). The sampling locations are in the northwest of the island where eclogitization is more localized than elsewhere.

nearly 50,000 km² in size, making the WGR one of the largest continental crust-dominated HP-UHP occurrences in the world. Amphibolite-facies retrogression is widespread and related to late- to post-orogenic, almost isothermal exhumation and transtensional deformation (Andersen, 1998; Terry and Robinson, 2003; Labrousse et al., 2004; Walsh and Hacker, 2004). Hints to the timing of the amphibolite facies overprint come from widespread 395 ± 2 Ma U–Pb sphene and zircon ages (Tucker et al., 2004, and references therein), consistent with Ar–Ar ages for low-Si muscovite between 399 Ma eastern parts of the WGR and <390 Ma further west (Hacker, 2007, and references therein).

Several lines of evidence suggest that the WGR was subducted and exhumed as a nearly coherent mass or at least in the form of a few large coherent crustal slices (cf. Andersen et al., 1991; Terry et al., 2000). This is indicated by a continuous increase of Caledonian eclogite facies P,T conditions towards the NW (e.g., Krogh, 1977; Cuthbert et al., 2000), by the regional SE–NW trend of amphibolite facies muscovite Ar–Ar ages (reviewed in Hacker, 2007), and large-scale consistency of structural grain (Krabbendam and Dewey, 1998; Labrousse et al., 2004).

A remarkable feature within the WGR is the spatially highly variable metamorphic grade of the prevalent litholo-

gies. Amphibolite-facies metabasites occur together with mafic granulites and HP- to UHP-eclogites on km to cm scales (e.g. Austrheim and Engvik, 1997; Engvik et al., 2000; Krabbendam et al., 2000; Wain et al., 2001). It has been shown that variability in the preserved metamorphic signature is due to heterogeneous strain and fluid ingress along the rocks' P, T evolution. Strain and fluid availability imposes kinetic control on rock and mineral reactivity, so that in absence of these factors assemblages can be metastably preserved even through episodes of extreme overstepping of equilibrium P, T conditions (Wayte et al., 1989; Austrheim, 1998; Krabbendam et al., 2000; Wain et al., 2001).

2.2. The Dalsfjord area

The WGR bedrock in the area around Dalsfjorden (Fig. 1) is mainly composed of granitoid gneisses and amphibolites, interlayered with metagabbros, chlorite harzburgites, pyroxenites, and eclogite bodies of varying sizes (Engvik et al., 2000, and references therein). Granulite facies, eclogite facies, and late-stage amphibolite facies rocks commonly occur in close contact with each other, in the same way as in the entire WGR and as exemplified on the here investigated island of Bårdsholmen (Fig. 1, inset).

Mylonites along the northern shore of Dalsfjorden were formed by top-W, exhumation-related shear along the Nordfjord-Sogn Detachment Zone (NSD; Norton, 1987; Andersen and Jamtveit, 1990). Available evidence suggests that this part of the WGR experienced near-UHP eclogite facies metamorphism. *P*, *T* work in the region resulted in estimates of 700 °C at ~23 kbar for eclogites in the Solund–Hyllestad–Lavik area (Hacker et al., 2003), some 20 km south of Bårdsholmen (Fig. 1). For the Drøsdal eclogite, ~8 km south of Bårdsholmen, Foreman et al. (2005) arrived at *T* = 720–830 °C and *P* = 19–21 kbar using the THERMOCALC multiequilibrium approach. Exchange reaction thermobarometry resulted in temperatures of 677 ± 21 °C and 691 ± 20 °C at pressures around 15 kbar for the Vårdalsneset eclogite body, Fig. 1 (Engvik and Andersen, 2000). In summary, conditions of 650 °C, 15–20 kbar appear to be a conservative minimum estimate of regionally attained eclogite facies conditions. Some regional *P*, *T* estimates for eclogite facies metamorphism, including those for Bårdsholmen eclogites, resulted in somewhat lower maximum temperatures (e.g. Engvik et al., 2000), an effect that can be attributed to uncertainties from estimating the ferric iron contents of clinopyroxenes (see Foreman et al., 2005; for discussion). The apparent inconsistencies in existing *P*, *T* estimates prompted us to revisit this topic (see below).

The age of eclogite facies metamorphism in the Dalsfjord area is not known with precision. As to the exhumation history, the available Ar–Ar muscovite dates from the wider study area (Chauvet and Dallmeyer, 1992; Berry et al., 1994; Fossen and Dallmeyer, 1998) are in line with the general view that amphibolite facies conditions persisted in the WGR of the area at least until 395 Ma.

3. SAMPLES AND SAMPLE PETROGRAPHY

Samples were collected from the northwestern edge of Bårdsholmen island, from a small stretch some 30 m along-shore (UTM: 6803575N, 294385E; Fig. 1, inset). In this area, both felsic and mafic rocks occur, and eclogitization is volumetrically more limited and more clearly confined to shear zones than elsewhere on the island. We investigated three macroscopically well-preserved granulites, and three samples of apparently well-equilibrated eclogites. Detailed data on assemblages in the samples are given in Table 1. Whole rock major and trace element compositions are presented in Table 2.

The granulite facies samples are two mafic rocks with fine- to medium grained equigranular texture and without

Table 2
Whole rock major element (in wt-%) and trace element (in ppm) compositions

Sample Rock type	B45 ecl	B11 ecl	B12–94 mg	BOR5 mg	BOR4 fg
SiO ₂	44.5	43.4	43.6	47.3	74.3
TiO ₂	3.18	2.97	3.18	2.61	0.02
Al ₂ O ₃	14.6	12.8	14.8	14.1	14.1
Fe ₂ O ₃	17.57	21.93	16.77	15.44	0.12
MnO	0.27	0.33	0.21	0.24	0.00
MgO	6.42	5.87	6.58	5.63	0.09
CaO	9.09	6.87	9.25	8.83	1.08
Na ₂ O	3.23	2.61	2.98	3.15	2.53
K ₂ O	0.58	0.84	1.07	1.41	6.73
P ₂ O ₅	0.49	0.69	0.51	0.45	0.03
H ₂ O	0.58	nd	0.72	0.68	0.38
CO ₂	0.12	nd	0.07	0.06	0.15
Sum	100.6	98.4	99.7	99.9	99.6
Ba	141	188	194	nd	1064
Cr	78	52	90	nd	<10
Ni	49	52	76	nd	<10
Rb	<10	24	<10	nd	179
Sr	65	138	192	nd	196
V	317	340	323	nd	<10
Y	52	49	50	nd	<10
Zn	145	156	119	nd	<10
Zr	211	227	211	nd	117

XRF data (GFZ Potsdam/RWTH Aachen). ecl, eclogite; mg, mafic granulite; fg, felsic granulite; nd, not determined.

any apparent foliation, dominated by feldspar (or its reaction products, see below), pyroxene and biotite (samples BOR5, B12–94). In addition, we investigated a coarse grained, non-foliated granulite consisting almost entirely of feldspar (BOR4). Microscopic investigation of the granulites shows that they all have been variably affected by the eclogite facies overprint. Even in the best-preserved granulites this overprint is seen as thin coronas around granulite facies phases and as newly-grown phases within plagioclase. Biotite, where in contact with plagioclase, is mantled by 20–50 µm thick coronas (Fig. 2a–d) made up of an inner garnet shell, occasionally surrounded by a second shell of omphacite. In detail, this omphacite may carry numerous, small needles of kyanite. This can be phenomenologically described, ignoring stoichiometry, as a reaction

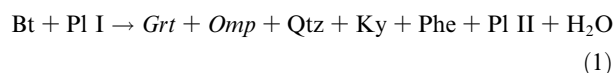


Table 1
Mineral assemblages of the investigated samples from Bårdsholmen

Sample Nr.	Granulite facies (primary)	Eclogite facies (secondary)
BOR5	Granulite Pl, Kfs, Opx, Cpx, Bt, Ilm, Ap, Zrn	Grt, Qtz, Ep, Rt
BOR4	Granulite Pl, Kfs, Qtz, Zrn	Phengite (traces)
B12–94	Granulite Pl, Kfs, Opx, Cpx, Bt, Am, Ilm, Mt, Ap	Grt, Omp, Ep, Ky, Rt
BOR2	Eclogite Zrn	Qtz, Grt, Omp, Phe, Rt, Mt
B11	Eclogite Zrn (?)	Omp, Grt, Am, Phe, Bt, Rt, Qtz, Py, Ap
B45	Eclogite Zrn (?)	Omp, Grt, Am, Phe, Bt, Rt, Qtz, Ap

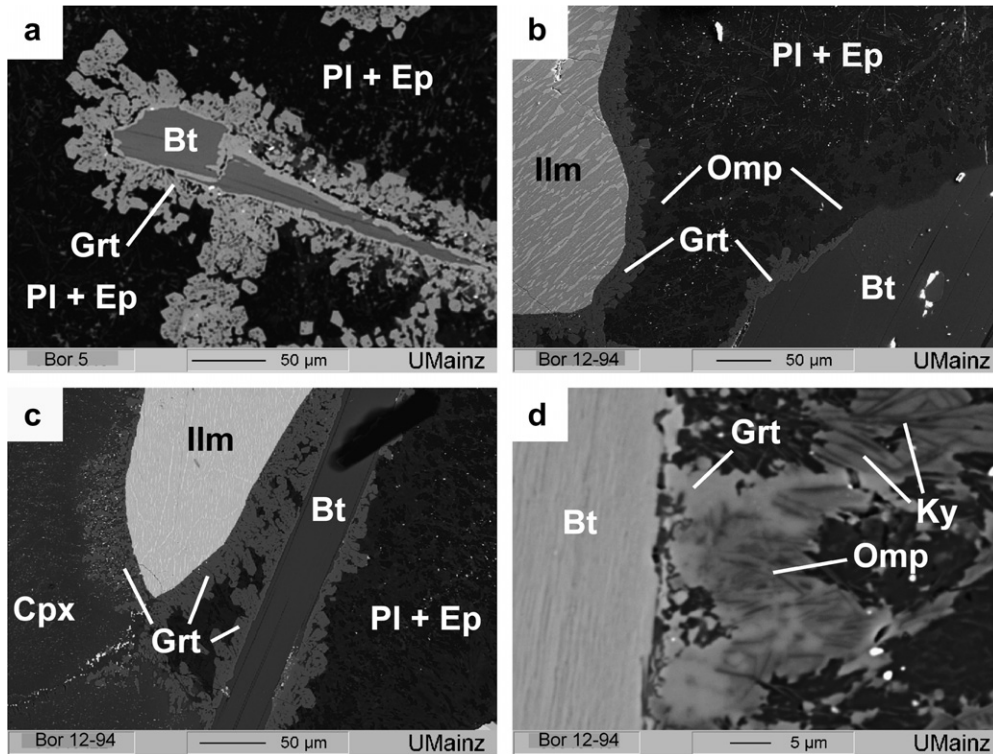


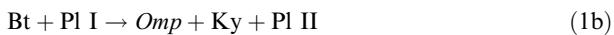
Fig. 2. BSE images of reaction textures in the mafic granulites (BOR5, B12-94) from Bårdsholmen. (a) Garnet rim around biotite. Plagioclase contains inclusions, consisting of needle-shaped epidote with minor garnet and omphacite. (b) Two-phase reaction rims (garnet and omphacite coronas) around ilmenite and biotite. Plagioclase contains numerous needle-shaped inclusions of epidote. (c) Garnet coronas around ilmenite and biotite. Note that garnet along the former ilmenite–clinopyroxene contact differs in appearance from garnet elsewhere. Transformation of plagioclase to a fine-grained intergrowth of epidote, garnet and omphacite is in an advanced stage here. (d) Close-up of a reaction rim on biotite, showing an inner rim of garnet, followed by an outer rim of omphacite containing small needles of kyanite.

(Main corona-forming phases in *italics*, abbreviations after Kretz, 1983; Phe, phengite).

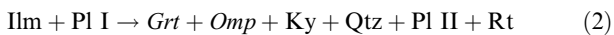
In cases where only garnets form the corona (Fig. 2a), the garnet often displays dendritic-like textures and is sub- to euhedral in shape. In general the garnet shells contain numerous inclusions of quartz.



In places biotites only show a thin, approximately 40 μm thick omphacite rim (Fig. 2b).



Ilmenite is mantled by similar corona sequences as biotite, usually with an inner shell of garnet and in places with an outer shell of omphacite (Fig. 2c). In general the garnet shell is more pronounced and thicker than in the coronas surrounding biotite.



Ilmenite may carry a one-phase garnet corona where it is in contact with clinopyroxene.



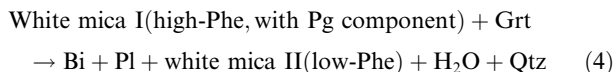
Granulite facies plagioclase is fully preserved only in the cores of large grains. Towards grain boundaries and along cracks, breakdown took place in presence of at least small

amounts of H_2O (released in reaction (1)). Here plagioclase appears loaded with numerous inclusions of needle-shaped epidote, but also tiny inclusions of garnet, omphacite and white mica are present.



Formation of these phases may have been facilitated by Fe, Mg present in solid solution within granulite-facies plagioclase, and does not imply large-scale mobility of these elements.

Eclogite facies samples are two fine-grained, slightly foliated, equigranular, mafic eclogites (B11, B45) and one quartz-dominated eclogite with a sparse, phengite-defined foliation (BOR2). This quartz-dominated sample was originally interlayered with moderately retrogressed mafic eclogites, and it appears that in the quartz-dominated assemblage, eclogite facies phases were protected from retrogression. Vein-like dark alteration zones, which are indicative of a post-eclogite-facies alteration and which are common in the WGR, were avoided as much as possible during sampling. Microscopically, there are no obvious relics in the eclogites from the granulitic stage, possibly apart from some zircon crystals. In sample B11 tiny biotite overgrowths on phengite and garnet indicate incipient eclogite breakdown, possibly due to reactions like



Indications for post-eclogite facies retrogression are rare to virtually absent in samples BOR2 and B45.

4. MINERAL CHEMISTRY

Quantitative mineral analyses used for thermobarometry, and backscatter electron images were performed on a JEOL JXA 8900 RL superprobe at the Institute for Geosciences at the University of Mainz. Natural and synthetic phases were used for calibration. Mineral analyses were performed with an accelerating voltage of 15 kV, a beam current of 12 nA and an electron beam diameter of 2 μ m. Apatites were analyzed with 15 kV acceleration voltage, 8 nA beam current and a beam diameter of 5 μ m. Obtained data were corrected for absorption, atomic number, fluorescence and background using the Phi-Rho-Z method (e.g., Pouchou and Pichoir, 1985). Representative mineral analyses are presented in Table 3

4.1. Pyroxene

The granulite facies samples (BOR5 and BOR12-94) contain both clino- and orthopyroxene. Granulitic clinopyroxene is classified as diopside and has the composition Wo₄₆En₃₆Fs₁₈. It has low Al₂O₃-contents resulting in low Al^{VI} values varying between 0.01 and 0.015. Mg/Mg + Fe ranges between 0.72 and 0.75. The corresponding orthopyroxene has a composition Wo_{<1.5}En₅₂Fs₄₇. The granulites also contain omphacitic pyroxene in corona textures between biotite or ilmenite and plagioclase. This omphacite has a variable jadeite component ranging from 24 to 52. In the eclogite samples (B11 and B45), omphacite has varying jadeite components (Jd_{31–39}) and is generally high in aegirine (Aeg_{15–20}).

4.2. Garnet

Garnet of all samples is generally rich in almandine. In the granulites (samples BOR5 and BOR12-94), garnet in coronas around biotite is Alm_{60–66}Gr_{s11–19}Prp_{10–18}Sps₄ and thus higher in almandine and lower in grossular than garnet from coronas around ilmenite (Alm_{44–48}Gr_{s44–49}Prp_{10–18}Sps₄). In the eclogites, the euhedral garnet contains less Sps component, and variations in garnet chemistry fall within a close compositional range. Garnet in sample B45 is Alm_{56–59}Gr_{s17–18}Prp₂₁Sps_{1.3–1.5} and displays only a very weak zoning in Alm content from core to rim, while garnet from sample B11 shows some zoning expressed in changing almandine and grossular components from core (Alm_{62–66}Gr_{s17–18}Prp_{18–19}Sps_{1–1.3}) to rim (Alm_{67–70}Gr_{s12–13}Prp_{16–20}Sps_{1–1.5}).

4.3. Sheet silicates

Biotite is present in both the granulite and eclogite samples. The reported #Mg = Mg/(Mg + Fe²⁺) values overlap and vary between 0.5 and 0.59. In the granulites, two chem-

ically slightly different types of biotite can be distinguished. Biotite showing overgrowths by Grt–Omp coronas displays high #Mg values (0.55 to 0.59), whereas low #Mg (0.5) usually characterizes biotite without coronas. In general no zoning with respect to Fe, Mg, Al, and K contents between biotite cores and rims was detectable by electron microprobe methods, neither at biotite–plagioclase nor at biotite–garnet interfaces. Phengite is present in the granulites only as tiny inclusions in converted plagioclase. In the eclogites it is abundant and has quite constant Si-contents of 3.4–3.45 and #Mg ranging from 0.73 to 0.77.

4.4. Amphibole

Green amphibole from the granulites is potassian pargasite (classification after Leake et al., 1997) with #Mg varying between 0.6 and 0.65. Amphiboles from the eclogites is magnesiottaramite showing lower #Mg (0.55) and higher Na(M4)- (ranging from 0.55 to 0.6) and higher Na(A) (0.6) contents than those found in the granulites facies pargasites.

4.5. Plagioclase

Plagioclase composition in the granulites varies strongly between An₂₀ and An₅₆. Highest An-contents in plagioclase is associated with lowest abundance of (eclogite facies) epidote needles.

4.6. Epidote

All analyzed epidote minerals occurring as needles within plagioclase are epidote (s.s.) with X_{P8} = Fe³⁺/(Fe³⁺ + Al) of 0.2.

4.7. Apatite

All analyzed apatite is fluor-apatite with F-contents varying between 2.77 and 4.3 wt%. It contains moderate amounts of Cl (0.11–0.51 wt%) and SrO (0.01–0.1 wt%). Chemical profiles across several apatite grains show no detectable zoning with respect to F, Cl and Sr contents. No chemical difference between apatite enclosed in feldspar and apatite situated on grain boundaries was detected by electron microprobe methods.

5. THERMOBAROMETRY

5.1. Granulite facies

Temperature estimates for the granulite facies metamorphism are based on Cpx–Opx thermometry, Al in Opx thermometry, and Opx–Bt thermometry. The Cpx–Opx calibrations of Wood and Banno (1973) and Wells (1977) yield results of 797–871 °C and 796–819 °C, respectively (Table 4). Temperatures calculated from core analyses of adjacent Opx–Bt pairs (Sengupta et al., 1990) give somewhat higher metamorphic temperatures of about 880 °C, in line with data obtained by the Ca in Opx thermometer (Brey and Köhler, 1990) which yield temperatures in the

Table 3
Representative electron microprobe analyses of minerals from granulite and eclogite facies rocks from Bårdsholmen

Sample	BOR5	BOR5	BOR5	BOR5	B11	B45	B11	B11	B45	B45	B11	B45
Rock	gran.	gran.	gran.	gran.	ecl.	ecl.	ecl.	ecl.	ecl.	ecl.	ecl.	ecl.
Phase	opx #45	cpx #46	bt #26	pl #36	omp #59	omp #108	grt #57r	grt #70c	grt #105c	grt #106r	phe #46	phe #103
SiO ₂	51.42	51.35	37.39	60.70	55.20	55.58	38.51	38.36	38.84	38.89	51.10	51.07
Al ₂ O ₃	1.10	2.37	14.09	25.72	8.32	8.55	21.82	21.50	21.70	21.99	23.79	25.81
TiO ₂	bd	0.28	4.90	0.02	0.03	0.03	0.01	0.02	0.05	0.02	0.68	0.51
Cr ₂ O ₃	0.02	bd	0.08	0.02	0.02	bd	0.02	0.06	bd	0.08	0.03	0.07
MgO	18.24	12.39	12.00	0.00	6.79	8.07	4.22	4.44	5.48	5.51	4.59	3.95
FeO	28.72	11.07	17.84	0.10	10.16	8.12	31.23	28.79	27.25	28.16	2.68	2.63
MnO	0.74	0.41	0.10	0.02	0.03	0.07	1.16	0.61	0.61	0.60	bd	0.03
CaO	0.51	22.42	0.00	4.58	10.85	12.58	4.82	7.52	7.16	6.09	0.03	0.03
Na ₂ O	0.07	0.62	0.09	8.85	8.33	7.48	0.02	0.03	0.02	0.06	0.16	0.23
K ₂ O	bd	bd	9.75	0.23	0.05	bd	0.02	bd	bd	0.02	10.17	10.45
Total	100.8	100.9	96.24	100.2	99.78	100.5	101.8	101.7	101.1	101.4	93.24	94.78
<i>Structural formulae</i>												
Si	1.95	1.91	2.81	2.69	1.98	1.98	5.99	5.98	6.00	5.99	3.49	3.43
Al ^{IV}	0.05	0.10	1.19	1.34	—	—	0.01	0.02	0.00	0.01	0.51	0.57
Al ^{VI}	—	—	0.06	—	0.35	0.36	3.99	3.91	3.95	3.99	1.40	1.48
Ti	0.00	0.01	0.28	0.00	0.00	0.00	0.00	0.00	0.01	0.00	0.04	0.03
Cr	0.00	0.00	0.00	0.00	0.00	0.00	0.00	0.01	0.00	0.01	0.00	0.00
Fe ²⁺	0.87	0.23	1.12	0.00	0.04	0.04	4.03	3.62	3.47	3.60	0.15	0.15
Fe ³⁺	0.05	0.11	—	0.00	0.27	0.21	0.03	0.11	0.05	0.03	—	—
Mn	0.02	0.01	0.01	0.00	0.00	0.00	0.15	0.08	0.08	0.08	0.00	0.00
Mg	1.03	0.69	1.34	0.00	0.36	0.43	0.98	1.02	1.26	1.27	0.47	0.40
Ca	0.02	0.89	0.00	0.22	0.42	0.48	0.80	1.25	1.18	1.01	0.00	0.00
Na	0.00	0.04	0.01	0.75	0.58	0.52	0.00	0.00	0.00	0.00	0.02	0.03
K	0.00	0.00	0.93	0.01	0.02	0.00	0.00	0.00	0.00	0.00	0.89	0.90

Gran., granulite; ecl., eclogite; omp, opx and cpx: formulae based on 4 cations; phengite and biotite: normalized to 11 oxygens; garnet: normalized to 16 cations; plagioclase: normalized to 8 oxygens; bd: beyond detection limit of ~0.01%.

Table 4
P, *T* estimates for granulite- and eclogite facies metamorphism, Bårdsholmen

Sample	Reference	<i>T</i> (°C)	<i>P</i> (kbar)
<i>BOR5 (granulite)</i>			
Opx–Bt	Sengupta et al. (1990)	865–899	
Opx–Cpx	Wood and Banno (1973)	797–871	
	Wells (1977)	796–819	
Ca in Opx	Brey and Köhler (1990)	841–871	(assumed 4 kbar)
		868–899	(assumed 10 kbar)
<i>B11 (eclogite)</i>			
Grt–Cpx ^a	Ellis and Green (1979)	808 [824]	(assumed 15 [20] kbar)
	Powell (1985)	789 [803]	(assumed 15 [20] kbar)
	Krogh (1988)	752 [769]	(assumed 15 [20] kbar)
	Ravna (2000)	758 [789]	(assumed 15 [20] kbar)
Grt–Phe–Cpx	Ravna and Terry (2004)	(assumed 600)	21.1–25.1
		(assumed 800)	23.1–27.7
<i>B45 (eclogite)</i>			
Grt–Cpx ^a	Ellis and Green (1979)	796 [811]	(assumed 15 [20] kbar)
	Powell (1985)	779 [791]	(assumed 15 [20] kbar)
	Krogh (1988)	741 [757]	(assumed 15 [20] kbar)
	Ravna (2000)	740 [770]	(assumed 15 [20] kbar)
Grt–Phe–Cpx	Ravna and Terry (2004)	(assumed 600)	21.1–26.0
		(assumed 800)	22.4–27.9
Grt–Phe–Cpx	Waters and Martin (1993)	(assumed 650)	20.5–23.0
		(assumed 750)	19.3–21.8

^a Average of 7 (sample B11) and 13 (sample B45) mineral pairs.

range 841–871 °C for assumed prevailing pressures of 4 kbar (Table 4). The above temperature estimates are consistent with those of Engvik et al. (2000) on similar samples. Unfortunately, the granulitic assemblages from Bårdsholmen do not allow for precise constraints on pressures reached during the granulite facies event.

5.2. Eclogite facies

Temperature estimation for the eclogite facies metamorphism using the Fe–Mg exchange between omphacite–garnet mineral pairs is complicated by the apparently high aegirine content (Fe³⁺) and correspondingly low Fe²⁺ contents of the analyzed omphacite as derived from charge balance considerations. Fe³⁺/Fe(total) ratios of omphacites calculated that way vary strongly between 0.68 and 0.95. Accordingly, temperature calculations based on the K_D (Fe²⁺–Mg) thermometer, using the Ravna (2000) Cpx–Grt calibration, yield unrealistically low metamorphic temperatures ranging from 220 to 500 °C (Fig. 4). Similar problems have been encountered also in other eclogites from the Dalsfjord area (Foreman et al., 2005). Therefore, temperature estimates based on the Cpx–Grt exchange thermometers were performed using the Ellis and Green (1979), Powell (1985), Krogh (1988) and Ravna (2000) calibrations for total iron partition coefficients (K_D (Fe_t–Mg)). Results range between 776 °C and 830 °C at 22 kbar for sample B11 and 764 °C to 818 °C for sample B45 (see Table 4 and Fig. 3b, c for details). Due to the missing data for ferric iron in the omphacite these data should be considered as maximum temperatures. However, if Fe³⁺/Fe_t ratios are plotted against estimated temperature using the K_D (Fe²⁺–Mg) a

regression line can be drawn through the obtained data points (Fig. 4). Extrapolating this line to the region of typically measured Fe³⁺/Fe_t ratios of eclogitic omphacites (Schmid et al., 2003), metamorphic temperatures >650 °C and up to >700 °C appear likely. Assuming a fixed Fe³⁺/Fe_t ratio of 0.4 well within the range of naturally measured ratios in omphacite (Schmid et al., 2003), calculated temperatures for the same omphacite–garnet pairs are 628–693 °C (sample B11) and 625–689 °C (sample B45), respectively.

Eclogite geobarometry using the inverse tschermaks exchange between garnet, clinopyroxene and phengite results in pressures of 19–21 kbar (after Waters and Martin, 1993) at 750 °C and 21–26 kbar at assumed 600 °C, or 23–27 kbar at 800 °C (following Ravna and Terry, 2004) (Fig. 3b and c).

5.3. Summary of PT data

Our *P*, *T* estimates of 800–900 °C for the granulite facies and of 19–25 kbar, 650–750 °C for the eclogite facies metamorphism are well within the reported range of *P*, *T* estimates from similar rocks in the Dalsfjord region (Engvik and Andersen, 2000; Hacker et al., 2003; Foreman et al., 2005), as summarized above. Specifically, all available evidence implies that during Caledonian subduction, conditions of >650 °C and ~20 kbar have been reached at a regional scale in the WGR.

6. ANALYTICAL PROCEDURES FOR ISOTOPE ANALYSES

Mineral separation for Rb–Sr and U–Pb analyses was carried out after careful removal of weathered and altered

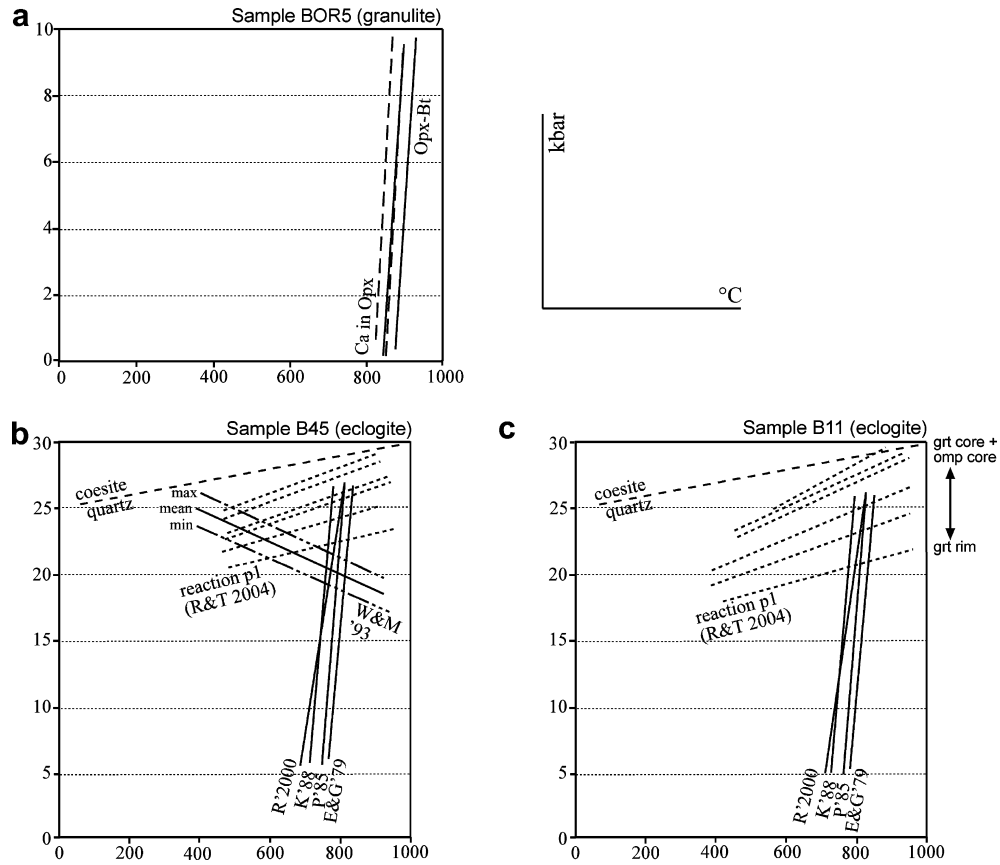


Fig. 3. PT diagrams showing the conditions for the main metamorphic events recorded in the Bårdsholmen rocks (a) P–T estimates for the granulite facies metamorphism (mafic granulites from Bårdsholmen). (b) and (c) Estimated P–T conditions for two eclogite samples from Bårdsholmen (compare with Table 2). R&T 04: Ravna and Terry (2004); R'2000: Ravna (2000); K'88: Krogh (1988); P'85: Powell (1985); E&G'79: Ellis and Green (1979); Ca in Opx: Brey and Köhler (1990); Opx–Bt: Sengupta et al. (1990); Opx–Bt: Sengupta et al. (1990); W&M '93: Waters and Martin (1993).

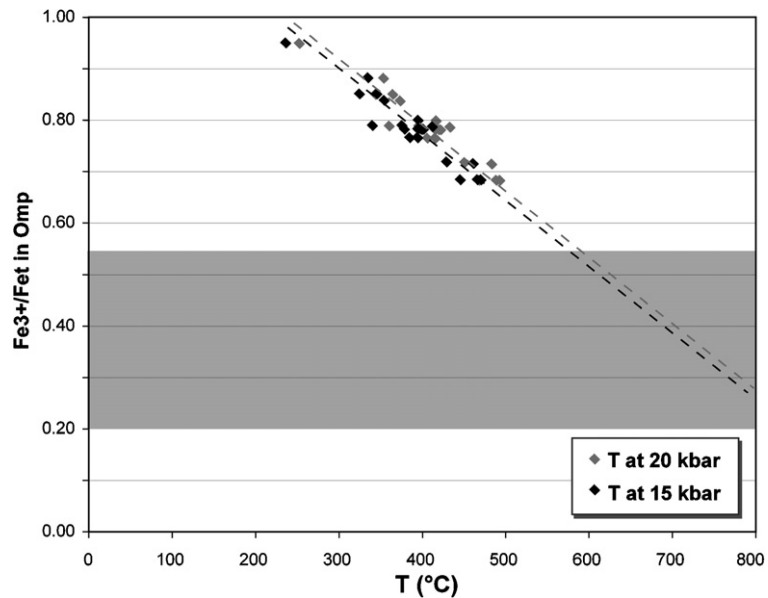


Fig. 4. Temperature calculated using the K_D (calculated Fe^{2+} –Mg), plotted against the corresponding $\text{Fe}^{3+}/\text{Fe}_t$ ratios in omphacite as obtained by charge balance considerations. The grey shaded area illustrates the typical range of measured $\text{Fe}^{3+}/\text{Fe}_t$ ratios as determined by Micro-XANES for omphacites from the Dabie Shan region (Schmid et al., 2003). See text for discussion.

parts of the samples. Samples for Rb–Sr analyses were small (10–100 g on average), to ensure sample homogeneity and to minimize the risk of isotopic gradients within the samples. Crushing was performed in a steel mortar, and followed by mineral enrichment using organic heavy liquids and a FRANTZ isodynamic separator. Mica sieve fractions were ground in pure ethanol in an agate mortar and then sieved again in ethanol to obtain inclusion-free separates. Secondary (Fe, Mn)-hydroxides observed on some omphacite, amphibole and garnet separates were removed with a 3% aqueous solution of oxalic acid as they are likely to adsorb contaminants. All mineral separates were finally checked and purified by hand-picking under a binocular microscope. For isotopic work, all Rb and Sr concentrations were determined by isotope dilution, using a set of mixed ^{87}Rb – ^{84}Sr spikes. Rb–Sr analytical data were generated on a VG Sector 54 multicollector thermal ionization mass spectrometer (TIMS) at GFZ Potsdam and processed following routines described in Glodny et al. (2002). The value obtained for $^{87}\text{Sr}/^{86}\text{Sr}$ of the NBS standard SRM 987 was 0.710266 ± 0.000014 (2σ , $n = 30$). Isochron parameters were calculated using the Isoplot/Ex program of Ludwig (1999), using a decay constant of $1.42 \times 10^{-11} \text{ a}^{-1}$ for ^{87}Rb as recommended by Steiger and Jaeger (1977). Standard errors, as derived from replicate analyses of spiked white mica samples, of $\pm 0.005\%$ for $^{87}\text{Sr}/^{86}\text{Sr}$ ratios and of $\pm 1.5\%$ for Rb/Sr ratios were applied in isochron age calculations (cf. Kullerud, 1991) except for the rare cases where determined analytical uncertainties were bigger than these values. Uncertainties of isotope data are quoted at 2σ throughout this work.

For U–Pb analysis, zircon grains free of inclusions were hand-picked under the binocular microscope, and then cleaned in warm, diluted HNO_3 and ultraclean H_2O . Zircon fractions from a granulite sample (BOR5) were also leached in hot Aqua Regia for 12 h to remove loosely bound U and Pb from possible pores and metamict zones. Zircon samples were put in Savillex™ teflon capsules together with a ^{205}Pb – ^{235}U mixed isotopic tracer and a mixture of concentrated HF– HNO_3 acids, then placed in a teflon insert into a Parr™ bomb, and heated for 3 days to 230 °C to achieve complete digestion. Standard ion exchange methods were used for chemical separation of Pb and U. Separates were loaded on single Re filaments. U and Pb isotopic analyses were conducted using a Finnigan MAT-262 at the GFZ Potsdam. The 2σ reproducibility of the NBS SRM-981 Pb isotopic standard is better than 0.1% for the $^{206}\text{Pb}/^{204}\text{Pb}$ and $^{207}\text{Pb}/^{204}\text{Pb}$ ratios, and corresponding uncertainties in $^{207}\text{Pb}/^{206}\text{Pb}$ ratios are $<0.06\%$. Laboratory blanks for the above procedure are <25 pg for Pb and <3 pg for U. Measured isotopic ratios were corrected by $0.11 \pm 0.05\%$ (2σ)/a.m.u. mass fractionation. Data reduction and age calculation was performed using the programs PBDAT (Ludwig, 1993) and Isoplot/Ex (Ludwig, 1999).

7. RESULTS

To date the granulite facies metamorphism, two zircon fractions from granulite BOR5 (leached in Aqua Regia) and four zircon fractions from the eclogite BOR2 were ana-

lyzed for their U–Pb systems. Zircons from the granulite are near-concordant, while the zircon fractions from the eclogite show variable degrees of discordance. Data regression yields a discordia line (MSWD = 10.4) with an upper intercept at 958 ± 7 Ma and a poorly defined lower intercept at 201 ± 93 Ma (Fig. 5 and Table 5). The weighted average $^{207}\text{Pb}/^{206}\text{Pb}$ age of the two zircon fractions from the granulite sample is 955 ± 3 Ma.

The three samples of eclogite facies rocks yield Rb–Sr multiminerall isochron ages of 403.9 ± 2.9 Ma (B11; $n = 6$, MSWD = 1.1) 403.2 ± 3.7 Ma (BOR2; $n = 4$, MSWD = 0.9), and 406.1 ± 5.3 Ma (B45; $n = 6$, MSWD = 12), all identical within limits of error (Table 6 and Fig. 6 a,b). The isochron ages are based on clearly unretrogressed phases of the eclogitic assemblages, i.e., phengite, garnet, omphacite, and zoisite. While in sample B11 biotite is isochronous with the other eclogite facies phases, it appears to be rejuvenated in sample B45. Both in sample B11 and B45 apatite plots slightly above the isochrons for the eclogitic assemblages and is excluded from isochron calculation. The weighted mean age for the three eclogites is 404.0 ± 2.1 Ma (2σ).

Granulite facies minerals from the partially eclogitized granulites reveal complex patterns in their Sr isotope mineral systematics. For these samples we prepared mineral concentrates of all accessible minerals, including several different grain size fractions of biotite, and several whole rock aliquots of $\sim 1 \text{ cm}^3$ each. Eclogite facies corona phases were not separable due to their small grain size. In separation of the granulite facies minerals, we took utmost care to analyze only transparent grains, to avoid contamination by adherent or intergrown eclogite facies reaction products. For sample B12–94, Rb–Sr mineral data plot around an 828 ± 17 Ma reference line (Fig. 6c). There is a clear correlation between grain size and apparent age for biotites: Large (355–500 μm) biotites yield a biotite-whole rock model age of 835 ± 12 Ma; smaller biotites yield progressively younger apparent ages down to 766 ± 12 Ma for the 125–180 μm sieve fraction (Table 7). The granulite facies phases amphibole, pyroxene and feldspar form, together with three whole-rock aliquots, a quasilinear array in an isochron diagram corresponding to an age of

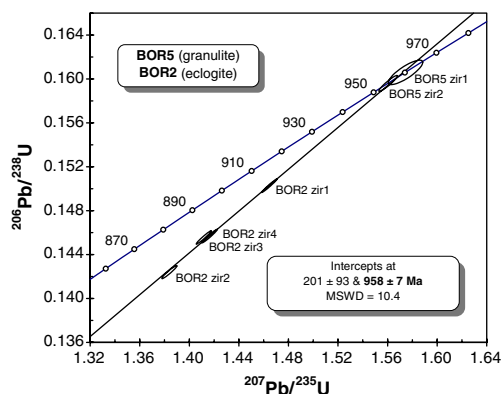


Fig. 5. U–Pb data for zircon from samples BOR5 (granulite) and BOR2 (eclogite).

Table 5
U–Pb analytical results

Fractions ^a	Weight (mg)		Concentrations		Measured		Atomic ratios ^d				Apparent ages (Ma)		Correl. coeff. ^e					
	U	Pb _{total} (ppm)	U	Pb _{com} ^b (ppm)	Pb _{com} ^b	²⁰⁶ Pb/ ²⁰⁴ Pb ^c	²⁰⁸ Pb/ ²⁰⁶ Pb	²⁰⁶ Pb/ ²³⁸ U	²⁰⁷ Pb/ ²³⁵ U	²⁰⁷ Pb/ ²⁰⁶ Pb	²⁰⁶ Pb/ ²³⁸ U	²⁰⁷ Pb/ ²³⁵ U		²⁰⁷ Pb/ ²⁰⁶ Pb	$\pm 2\sigma$	$\pm 2\sigma$		
Sample BOR 5																		
P5837	zr1	<90 br AR	0.324	294	55.5	449.5	0.1327	0.16060	0.57	1.5745	0.72	0.07111	0.41	960.1	960.2	960.4	8.4	0.822
P5838	zr2	>90 br AR	0.244	308	52.7	1538	0.1286	0.15959	0.37	1.5604	0.39	0.07091	0.13	954.5	954.6	954.9	2.7	0.943
Sample BOR 2																		
P5945	zr1	cl fr els	0.510	508	76.1	2114	0.0562	0.15028	0.34	1.4646	0.35	0.07068	0.06	902.5	915.9	948.3	1.3	0.983
P5946	zr2	>200 tu br	0.581	969	143	768.0	0.0414	0.14240	0.34	1.3839	0.35	0.07049	0.10	858.2	882.1	942.5	2.0	0.962
P5947	zr3	y cl p	0.586	549	81.5	1112	0.0502	0.14556	0.34	1.4116	0.35	0.07034	0.08	876.0	893.8	938.2	1.6	0.974
P5948	zr4	br pr id	0.565	762	113	6.95	0.0445	0.14569	0.35	1.4164	0.36	0.07051	0.08	876.7	895.8	943.2	1.7	0.973

^a Codes in the fraction numbers are zir, zircon. Abbreviations are: 30–100, >200 = size fractions (μm); AR, etched in aqua regia for ~12 h; tu, turbid; cls, colorless; id, idiomorphic; p, prismatic; y, yellowish; br, brownish; fr, fragments.

^b Total common Pb in sample (initial Pb + blank).

^c Data corrected for fractionation, and common lead in tracer.

^d Corrected for fractionation, procedural laboratory blanks (<25 pg Pb, 3 pg U), and initial common Pb, calculated following the model of Stacey and Kramers (1975). Pb fractionation correction is 0.1‰/amu ($\pm 0.05\%$ 2σ). 2σ uncertainties on the isotopic ratios are calculated with the error propagation procedure of Ludwig (1980).

^e Absolute error, in Ma.

^f ²⁰⁷Pb/²³⁵U/²⁰⁶Pb/²³⁸U error correlation coefficient.

919 ± 43 Ma ($n = 6$, MSWD = 4; Fig. 6d). This age value is identical within error with the age for granulite facies metamorphism as obtained from zircon U–Pb data (955 ± 3 Ma, see above). The Rb–Sr data for apatite plot significantly above the regression line (Fig. 6d).

For the granulite sample BOR5 we obtained a very similar data pattern. Again there is a clear correlation between biotite grain size and biotite-whole rock model ages, with the highest age value of 729 ± 11 for biotites >500 μm and lower values down to 669 ± 10 Ma for the smallest (180–250 μm) separated biotites (Fig. 6e and Table 7). Isochron age calculation using the data for amphibole, feldspar and two whole rock aliquots results in an age of 955 ± 94 Ma ($n = 4$, MSWD = 3.6; Fig. 6f), an age value again identical with the age of granulite facies metamorphism. As it is the case for the other sample, apatite plots significantly above that regression line.

8. DISCUSSION

8.1. Age of granulite facies metamorphism

The weighted mean ²⁰⁷Pb/²⁰⁶Pb age of 955 ± 3 Ma for the zircons of the granulite sample BOR5 coincides within error with U–Pb data for several gneiss and migmatite samples from adjacent areas of the southern WGR (Skår and Pedersen, 2003; Røhr et al., 2004). Skår and Pedersen (2003) reported an age of 969 ± 8 Ma, based on U–Pb zircon data that is backed up by similar U–Pb age data for titanite, indicating a prolonged phase of high heat flow and metamorphism as the dominant regional Sveconorwegian high-temperature event. Cathodoluminescence images of zircon from the granulite facies sample BOR5 show weak sector or patchy zoning, oscillatory zoning is ghostly in appearance and rarely observed, and many zircon grains are CL-featureless, all observations typical for metamorphic zircon (Vavra et al., 1999; Hoskin and Black, 2000). Similar zircons are found in the eclogite sample BOR2. However, these zircons, discordant in their U–Pb systematics, in addition show spectacular replacement-recrystallization domains, nucleating from cracks and grain boundaries (Fig. 7a–c). Newly grown or recrystallized zircon is recognized from CL-brightness. Similar zircon CL patterns have been described from the Bergen Arcs eclogites, Norway (Bingen et al., 2004), which experienced a similar metamorphic history. The discordia upper intercept age of 958 ± 7 Ma (Fig. 5) is, within error, identical to the weighted mean ²⁰⁷Pb/²⁰⁶Pb age of 955 ± 3 Ma for zircons from the granulite sample, which we interpret as dating granulite facies zircon crystallization. The main reason for discordancy of the zircons from the eclogite sample appears to be the Caledonian metamorphic imprint at ~400 Ma. Additional reasons for discordance probably include some post-Caledonian or recent Pb loss, as the lower intercept age of 201 ± 93 Ma is not in line with the known age of the Caledonian metamorphic overprint. It is worth noting that the degree of eclogite-facies imprint on the zircon, as evident both from CL images and from the isotopic data, is correlated with the eclogite-facies reaction progress in their host rock: the slightly reacted granulite carries

Table 6
Rb/Sr analytical data

Sample No. Analysis No.	Material	Rb (ppm)	Sr (ppm)	$^{87}\text{Rb}/^{86}\text{Sr}$	$^{87}\text{Sr}/^{86}\text{Sr}$	$^{87}\text{Sr}/^{86}\text{Sr}$ $2\sigma_m$ (%)
<i>Eclogite facies assemblages</i>						
B11 (403.9 ± 2.9 Ma (excl. apatite); MSWD = 1.1, $\text{Sr}_i = 0.716880 \pm 0.000031$)						
PS710	wm $m = 0.5\text{--}0.7$ A	337	91.6	10.7	0.778725	0.0012
PS714	wm >250 μm	345	85.7	11.7	0.783729	0.0014
PS718	wm 125–160 μm	329	107	8.92	0.768160	0.0018
PS717	Garnet	2.76	16.4	0.488	0.719723	0.0014
PS719	Omphacite	1.35	96.2	0.0405	0.717099	0.0016
PS722	Biotite	444	13.4	101	1.301848	0.0012
PS715	Apatite	0.13	7125	0.00005	0.717749	0.0018
BOR2 (403.2 ± 3.7 Ma, MSWD = 0.9, $\text{Sr}_i = 0.712273 \pm 0.000035$)						
PS738	wm 250–500 μm nm 0.42 A	188	263	2.07	0.724178	0.0016
PS741	wm >500 μm	188	261	2.09	0.724377	0.0018
PS743	Zoisite	13.3	7827	0.00493	0.712301	0.0016
PS744	wm 250–500 μm m = 0.42 A	198	283	2.03	0.723824	0.0014
B45 (406.1 ± 5.3 Ma (excl. biotite and apatite); MSWD = 12, $\text{Sr}_i = 0.70769 \pm 0.00017$)						
PS733	wm >250 μm	207	52.8	11.4	0.773881	0.0014
PS728	wm 125–160 μm	204	54.0	11.0	0.771638	0.0014
PS737	wm 160–250 μm	202	59.4	9.90	0.764703	0.0014
PS709	Omphacite	2.02	49.8	0.118	0.708317	0.0016
PS749	Whole rock	13.0	71.3	0.529	0.710906	0.0016
PS713	Garnet	1.31	8.28	0.459	0.710242	0.0018
PS729	Apatite	0.41	3034	0.00039	0.708230	0.0016
PS736	Biotite >100 μm	259	11.0	70.5	1.100973	0.0012
<i>Granulites with partial eclogitization</i>						
B12–94 (919 ± 43 Ma, MSWD = 4, $\text{Sr}_i = 0.704728 \pm 0.000080$; excl. apatite and biotite); 828 ± 17 Ma (all data)						
PS706	Apatite	0.29	393	0.00216	0.705486	0.0016
PS708	Feldspar (clear)	0.85	538	0.00457	0.704761	0.0014
PS716	Amphibole	6.45	75.8	0.246	0.707981	0.0018
PS720	Pyroxene	0.07	4.26	0.0478	0.705404	0.0016
PS707	Biotite >250 μm	236	8.44	89.4	1.771833	0.0016
PS711	Biotite <250 μm	234	11.8	61.4	1.417986	0.0014
PS751	Biotite 355–500 μm	240	8.63	88.9	1.765272	0.0020
PS752	Biotite 125–180 μm	232	19.8	35.1	1.088750	0.0034
PS850	Whole rock 1 (1 cm^3)	7.80	232	0.0971	0.706018	0.0014
PS853	Whole rock 2 (1 cm^3)	10.1	225	0.130	0.706439	0.0014
PS747	Whole rock 3 (1 cm^3)	11.3	226	0.144	0.706569	0.0016
BOR5 (955 ± 94 Ma, MSWD = 3.6, $\text{Sr}_i = 0.7085 \pm 0.0019$; excl. apatite and biotite); 689 ± 25 Ma (all data)						
PS972	Biotite >500 μm	689	8.22	322	4.043412	0.0076
PS806	Biotite 355–500 μm	780	8.13	383	4.578559	0.0010
PS825	Biotite 250–355 μm	796	7.21	459	5.177935	0.0010
PS823	Biotite 180–250 μm	797	7.20	457	5.073682	0.0010
PS818	Amphibole	22.1	50.9	1.26	0.725379	0.0014
PS851	Whole rock 1 (1 cm^3)	64.2	178	1.05	0.722977	0.0014
PS854	Whole rock 2 (1 cm^3)	65.2	152	1.24	0.725488	0.0016
PS1062	Feldspar (clear)	367	484	2.20	0.738581	0.0014
PS816	Apatite	0.82	300	0.00788	0.721035	0.0012
BOR4 (664 ± 40 Ma, MSWD = 0.4, $\text{Sr}_i = 0.7318 \pm 0.0014$)						
PS726	Feldspar white	207	279	2.15	0.752111	0.0016
PS734	Feldspar rose	284	272	3.04	0.760474	0.0018
PS748	Whole rock	181	200	2.63	0.756798	0.0014

An uncertainty of ± 1.5% (2σ) is assigned to Rb/Sr ratios. wm, white mica; m/nm, magnetic/nonmagnetic on Frantz magnetic separator, 13° inclination, at electric current as indicated. Typical sample weights are 0.5–5 mg for apatite and epidote minerals; 5–15 mg for feldspar, amphibole, white mica, biotite; and 15–50 mg for pyroxenes and garnet.

nearly unaffected zircon, while in the fully reacted eclogite the zircon is significantly overprinted. This shows that zircon reworking is not only a function of metamorphic tem-

peratures. Instead, fluid- and deformation-assisted metamorphic reaction in a rock appears to be the critical factor.

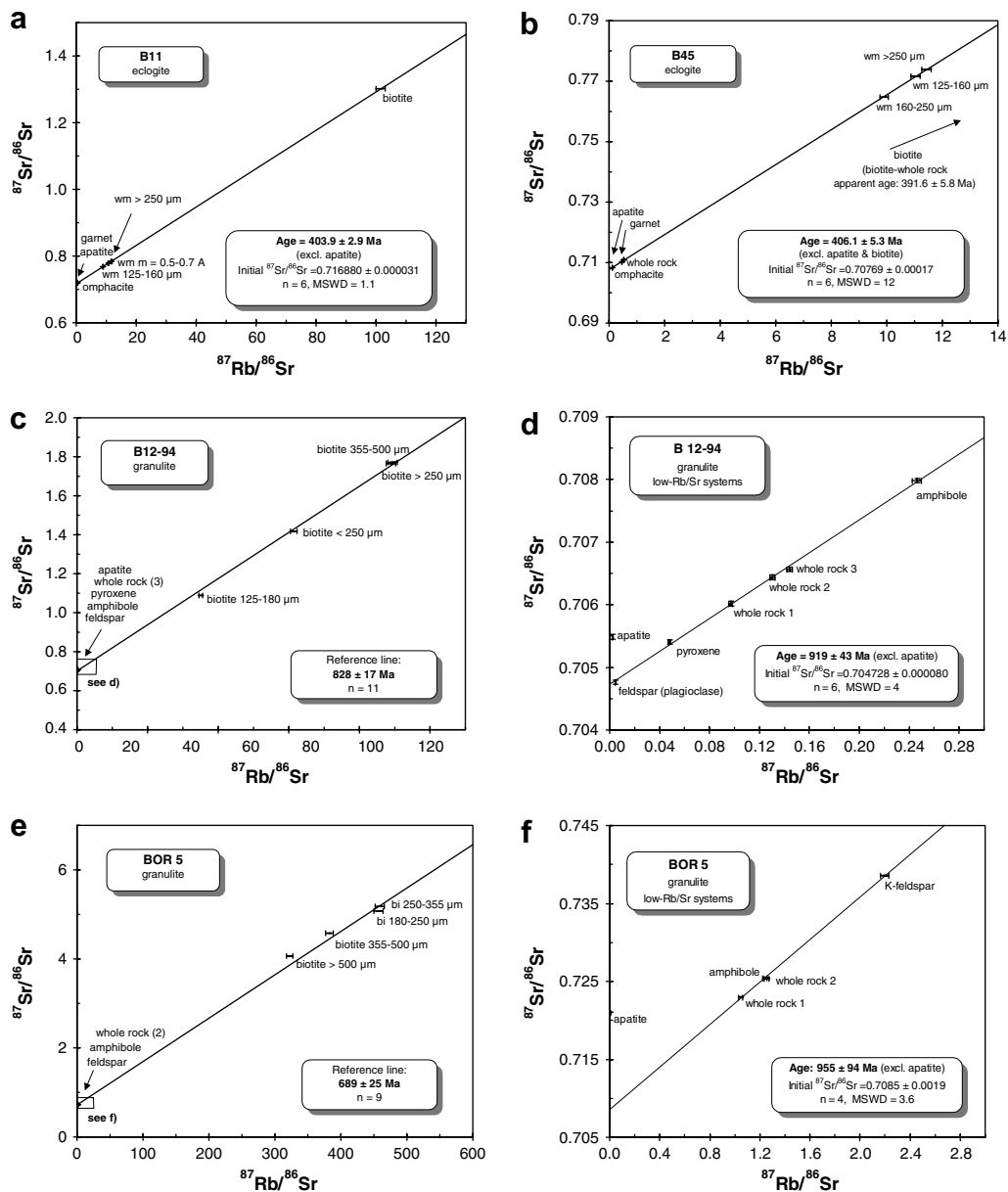


Fig. 6. Rb–Sr isotopic data for eclogites and partially eclogitized granulites from Bårdsholmen. Analytical data: see Table 6. Abbreviations: wm, white mica; bi, biotite; m: magnetic (Frantz separator) at 13° inclination, and electric current as indicated.

8.2. Age of eclogite facies metamorphism

Three multiminerall Rb/Sr internal isochrons from Bårdsholmen eclogites yield concordant ages (samples B11, BOR2, B45; Fig. 6, Table 6), with a weighted mean age of 404 ± 2 Ma. It has been shown that initial Sr-isotopic equilibria among all eclogite facies phases, together with absence of a positive correlation between apparent age and grain size for mica, are sufficient criteria to interpret such multiminerall isochron data as eclogitization ages (Glodny et al., 2002; Glodny et al., 2005). Grain size vs. age correlations for phengite are not observed in the dataset from the eclogites (Fig. 6). However, in samples B11 and B45 not all phases co-define the mineral isochrons: apatite plots above

the isochron lines in both examples, while biotite co-defines the isochron age only in sample B11. Internal, intermineral isotope exchange by diffusion during post-eclogite facies prolonged cooling would preferentially affect the two phases with the comparatively highest Sr diffusivities (sensu Giletti, 1991; apatite and biotite). The fact that in only one sample biotite appears rejuvenated, while chemical compositions (Table 2), modal abundances of biotite and apatite, as well as rock textures of the two samples are similar, suggests that other factors than posteclogitic prolonged cooling are responsible for the observed disequilibria. These factors may be either the slight amphibolite- to greenschist-facies alteration, or incipient weathering (cf. Jeong et al., 2006). In any case, since Sr-isotopic signatures of

Table 7
Biotite apparent ages

Sample	B12–94	BOR5
<i>Sieve fraction</i>		
>500 μm		729 \pm 11 Ma
355–500 μm	835 \pm 12 Ma	708 \pm 10 Ma
250–355 μm		682 \pm 10 Ma
>250 μm	836 \pm 12 Ma	
<250 μm	813 \pm 12 Ma	
180–250 μm		669 \pm 10 Ma
125–180 μm	766 \pm 11 Ma	

Apparent ages calculated for biotite–whole rock pairs (see Table 6; whole rock analysis PS853 for sample B12–94, analysis PS851 for sample BOR5). Sieve fractions >500 μm and >250 μm include all grain sizes up to the maximum biotite grain size in the rock (\sim 700 μm).

the critical eclogite facies phases omphacite, zoisite, phengite and garnet are consistent with full isotopic equilibration of the rocks during metamorphism we interpret the age of 404 ± 2 Ma as dating eclogitization, at P , T conditions as recorded by the thermobarometric data for these eclogites. This new 404 ± 2 Ma multimineral Rb/Sr age from the southern WGR is in excellent agreement with high-precision age data for near-peak eclogite facies metamorphism in the central, UHP parts of the WGR between Nordfjord and Hareidland, namely with U–Pb zircon data of 405–400 Ma for a Flatraket eclogite (Root et al., 2004), with a 402 ± 2 Ma zircon age from Hareidland (Carswell et al., 2003b; Tucker et al., 2004), with a 408 ± 7 Ma Sm/Nd isochron age from Saltaneset, Outer Nordfjord area (Carswell

et al., 2003a), and with two Sm–Nd mineral ages from Vigra (402.7 ± 4.6 Ma) and Gurskøy (398.3 ± 5.5 Ma), Sørøyane area (Kylander-Clark et al., 2007). This concordancy of eclogite facies ages testifies to both coherency of the central and southern WGR during subduction, and to the reliability of the available Rb/Sr, Sm/Nd and U–Pb geochronological data.

8.3. The role of fluids, deformation and diffusion for reaction progress

Eclogitization of granulite on Bårdsholmen is controlled by fluid availability. This is obvious from the field observation that full eclogitization of granulite scale-invariably occurs only along fluid pathways like cracks, veins, and deformation zones. Reaction progress diminishes with distance to fluid pathways (Austrheim and Engvik, 1997; Engvik et al., 2000). Nearly identical major and trace element compositions for mafic granulites and mafic eclogites on Bårdsholmen (Table 2) suggest that even near the fluid pathways the overall amount of fluids involved in eclogitization was small, and unable to cause any detectable element mobilization. The near-isochemical (exception: H_2O) conversion of granulite to eclogite further testifies that reaction progress was controlled by deformation and fluid availability, rather than by rock composition. The fact that large proportions of the original granulite were metastably preserved through eclogite-facies metamorphism indicates that the rock volume now forming Bårdsholmen was overall fluid-deficient during eclogite facies conditions. This is corroborated by the finding that eclogitization was largely due to the infiltration of water-rich fluids from external

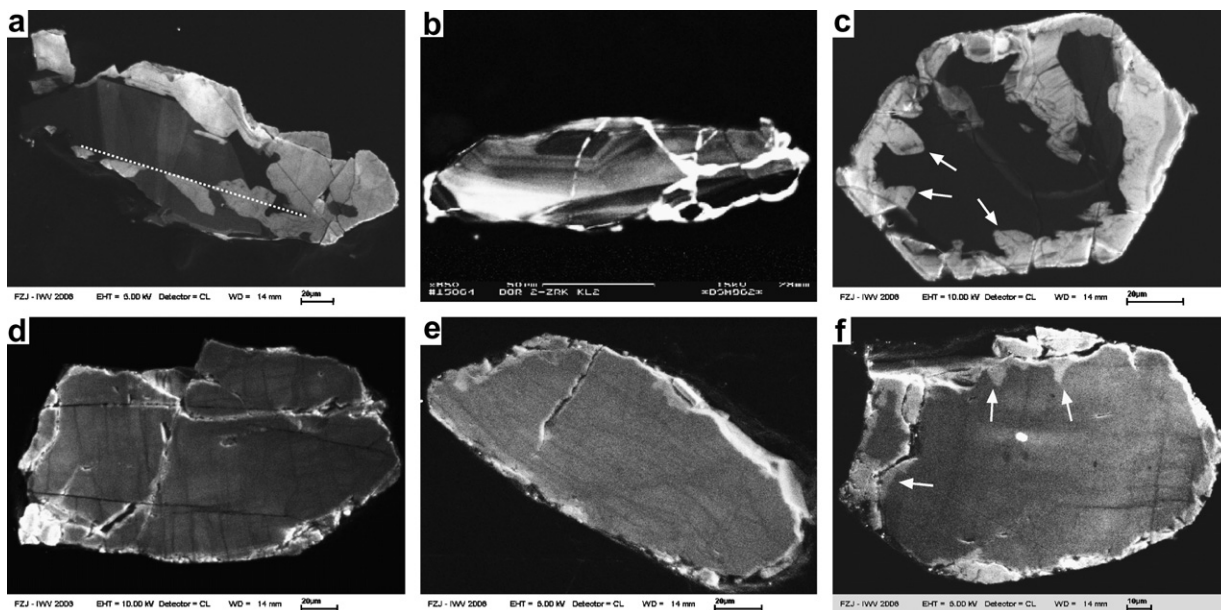


Fig. 7. Cathodoluminescence images documenting alteration associated with eclogite facies metamorphism. (a–c) Zircon crystals from sample BOR-2. Note CL-bright recrystallized domains along crystal rims and sealed cracks. Stippled line in (a) marks position of a sealed crack. Arrows in (c) point to ‘crystal-like’ recrystallization domains nucleating at the grain boundary. (d–f) Apatite grains from the partially eclogitized granulite of sample BOR-5. Note numerous small, CL-dark, sealed cracks. Arrows in (f) point to CL-bright domains, apparently invasively growing from the grain boundaries.

sources, and that H₂O was internally consumed by the eclogitization reactions, leaving behind residual brines rich in highly incompatible elements, like Br and Pb (Svensen et al., 1999; Svensen et al., 2001). For the fairly well preserved granulites this means that the eclogitization reactions stranded at low reaction progress, due to full consumption of free fluids shortly after the rocks' exposure to eclogite facies *P*, *T* conditions. Since then, these rocks must have remained devoid of free aqueous fluids, i.e., 'dry' until their final exhumation.

The small degree of eclogitization visible in the granulites distal to fluid pathways is caused by two factors. Small amounts of initially free H₂O, possibly from fluid inclusions (cf. Philippot and Selverstone, 1991), were consumed mainly by the formation of epidote–zoisite within feldspar. Further, H₂O released during incipient biotite breakdown reactions, was subsequently consumed by formation of phengite and epidote. More importantly, diffusion-controlled solid state reaction is evident from the 'coronitic' reaction textures (Fig. 2). The appearance and phase composition of metamorphic reaction rims, e.g. around biotite (Fig. 2), is controlled by the local environment, namely by local grain boundary geometries and the immediately neighboring granulitic phases. This local control on metamorphic reaction products is incompatible with presence of free fluids during reaction, which would have enabled rapid transport of reaction components along grain boundaries thus eliminating the close geometric correlation between reactant phases and reaction products. We therefore take the local peculiarity of reaction products as a strong indication for diffusion-driven solid state reactions (Mørk, 1985; Gilotti and Elvevold, 1998), either without or with only very limited participation of fluids. The local control on reaction rim microtextures further corroborates a conclusion by Joesten (1991) that rapid diffusion along grain boundaries is not the dominant mechanism of mass transport during metamorphism. It is stressed that combined volume and grain boundary diffusion during eclogite facies conditions only caused growth of reaction rims a few μm wide and with a very fine-grained, high-free-energy, nonequilibrium structure (Fig. 2). Time-integrated diffusion of major elements at fluid-absent conditions was thus a phenomenon restricted to the $<100 \mu\text{m}$ scale.

8.4. Sr redistribution in a dry system

In the above paragraph it was shown that textures in the partially eclogitized granulites provide evidence that most of the visible eclogitization was a consequence of fluid-absent diffusion. After incipient eclogite facies consumption of small amounts of free fluids, the rocks have been dry (i.e., devoid of free fluids) during all their passage through the Caledonian high-temperature, eclogite-facies and amphibolite facies segments of their *P*–*T* path. The geochronologic context, as outlined above, indicates that the rocks experienced at least 5–10 Ma of $T > 500 \text{ }^\circ\text{C}$, between $404 \pm 2 \text{ Ma}$ for eclogitization, and amphibolite facies conditions at $\sim 395 \text{ Ma}$. The patterns of Sr isotope distribution observed in these granulites should thus be characteristic for the effects of long-term, solely temperature-driven diffu-

sion, because here recrystallization-inducing processes demonstrably did not occur.

The most striking features evident from the isochron diagrams for the granulite samples are (i) isotopic disequilibria, e.g., between apatite, biotite, and feldspar; (ii) nearly preserved isochron correlations between the granulitic phases pyroxene, amphibole, feldspar (K-feldspar and plagioclase), and cm^3 -sized whole rock aliquots (Fig. 6d and f), (iii) the incomplete Caledonian-age reset of biotite Rb–Sr signatures, associated with systematic positive correlations between biotite crystal size and apparent biotite-whole rock 'age' (Fig. 6c, e, and Table 7) and (iv) the systematic presence of 'excess' radiogenic Sr in apatite (Fig. 6d and f).

Diffusivities of Sr in individual phases of the assemblage are the key to a qualitative understanding of diffusion-induced disequilibrium patterns. A literature survey for tracer diffusion data for the individual minerals of the granulitic assemblage reveals that at dry conditions and eclogite facies temperatures, Sr diffusivity within biotite is highest (cf. Jenkin, 1997), followed by apatite (Cherniak and Ryerson, 1993). Lower Sr diffusivities characterize alkali feldspar (Giletti, 1991), plagioclase (Giletti and Casserly, 1994), and amphibole (Brabander and Giletti, 1995). The lowest Sr diffusivities are reported for pyroxene (Sneeringer et al., 1984). This sequence is also in line with theoretical predictions for cation tracer diffusivities based on ionic porosity concepts (Fortier and Giletti, 1989; Dahl, 1997). Given the above sequence of diffusivities, it is anticipated that if any closed-system diffusional isotope exchange between minerals occurs, the mineral pair with highest Sr diffusivities will be affected most (cf. Giletti, 1991; Eiler et al., 1992). In comparison to this mineral pair, other phases will be less involved in exchange processes, or even remain virtually inert, as dictated by their relative diffusivities. The preservation of the Sveconorwegian isochron correlation between pyroxene, amphibole and feldspar in the granulites B12–94 and BOR5 in fact demonstrates that these more refractory phases record their original isotopic signature and consequently were not affected by isotopic exchange. In the here studied assemblage, the preferred mode of inter-mineral Sr transfer thus has been between apatite and biotite, with a grain-size correlated decrease of the $^{87}\text{Sr}/^{86}\text{Sr}$ ratio in biotite and a corresponding increase in apatite. Such a behavior of these two minerals during closed-system inter-mineral Sr isotope exchange in a natural rock has in parts already been theoretically predicted by Giletti (1991). The new isotopic data are well in line with these conjectures. The clear and reproducible grain size vs. age correlation for biotite (Table 7) is compatible with bell-shaped distributions of apparent Rb–Sr ages within biotite, as expected from diffusion theory. The correlation further suggests that the effective diffusion domain size of the biotite is, in the here studied case, in fact identical to the observed biotite grain size. For the apatite it is an open question whether Sr exchange was by bulk volume diffusion. Cathodoluminescence imaging (Fig. 7d–f) of apatite from granulite sample BOR5 reveals a network of planar features, possibly resembling former cracks, which may have defined apatite diffusion domain sizes.

It has been known since long that apatite can exchange Sr preferentially with micas by diffusion (e.g., Baadsgaard and Van Breemen, 1970). More recent studies of Sr isotope systematics in rock systems with solely diffusion-controlled isotope exchange reveal Sr redistribution patterns strikingly similar to the one observed here. Tilton et al. (1997) have shown that in a metagranite from the Dora Maira, Western Alps, Sr signatures in feldspar were preserved through temperatures >700 °C at UHP conditions, while biotite shows only partial rejuvenation and apatite exhibits large proportions of ‘excess’ radiogenic Sr. Similar observations were made in statically heated ultramafic rocks from the Bergen Arcs, Norway (Kühn et al., 2000). We therefore conclude that the disequilibrium Sr isotope distribution pattern observed in the samples from Bårdsholmen, with an only partial diffusional re-equilibration affecting preferentially the two phases with the highest Sr diffusivities in the rock, is characteristic in a general sense for diffusion-controlled isotope exchange. It is worth noting that the present case study deals with a setting of static, fluid-absent *re-heating* of assemblages, which did not result in re-equilibration of Sr isotopes between the minerals. We anticipate that in a situation of static, fluid-absent, *monotonous cooling* from a stage of full isotopic equilibrium (the scenario which Dodson (1973) considered for his theory of isotopic closure) an essentially similar Sr isotope disequilibrium distribution pattern would develop. In this case disequilibria would be the more pronounced the slower cooling proceeded, but in rapidly cooled rocks possibly undetectable with today's analytical techniques.

In detail, the result of solely diffusive Sr isotope redistribution in a polymineralic rock depends on multiple factors including mineral modal abundances, grain sizes and shapes, diffusivities, transport properties of the intergranular space, and the thermal history. However, it will *generally not lead to equilibrium* among all phases of a rock, as demonstrated in analogy for stable isotope diffusion (Eiler et al., 1992). It appears that a geochronological evaluation of a strictly diffusion-related Sr isotope distribution pattern (which is a priori a disequilibrium pattern, as observed in the granulite samples) is virtually impossible. Any thermo-chronological evaluation of a truly diffusion-governed Sr isotope distribution pattern would require as an input parameter, among others, exact data on the μm scale for the spatial distribution of Sr isotopes in all minerals of a rock, i.e., information that is up to now analytically inaccessible. Taken more simply, if closed-system, diffusion-controlled intermineral isotope exchange occurred in a rock, a ‘thermo-chronological’ interpretation of isotopic data is a priori incorrect. This is immediately clear from the Rb–Sr biotite data of the granulite samples (Table 7). Neither do the apparent biotite-whole rock data, scattering between 836 and 669 Ma, date cooling below any kind of ‘closure temperature’, nor do they have a direct geochronological meaning at all.

8.5. Isotope redistribution: the role of apatite

As shown above, the Sr reservoir of apatite may act as an exchange partner in a closed rock system for Sr liberated

by high-diffusivity phases like the micas. In fluid-absent systems apatite thus is a valuable monitor for occurrence of any diffusional exchange, i.e., partial isotopic/age resetting, between mica and its surroundings. Preserved initial Sr-isotopic equilibrium between apatite and low-diffusivity phases like the pyroxenes indicates that diffusional redistribution of radiogenic Sr within a rock was negligible. However, this argument cannot be inverted. It appears that the Sr isotopic signature of apatite can be altered even if no significant diffusional release of radiogenic Sr from the micas ever occurred. Such a situation is seen in sample B11 (eclogite), where apatite plots significantly above the isochron line (403.9 ± 2.9 Ma) defined by all other phases *including biotite*. It remains unclear where the apparent ‘excess’ radiogenic Sr in apatite came from, whether from the minute amphibolite—to greenschist facies overprint in that sample, or from external sources. Several studies have shown that in presence of fluid, apatite may recrystallize and change its isotope budget even in very low-temperature settings, down to <150 °C (Romer, 1996), possibly by Cl/F/OH exchange with fluids out of equilibrium with the apatite (e.g., Smith and Yardley, 1999). Therefore, Sr-isotopic disequilibrium between apatite and other phases is an unequivocal indicator of diffusional isotope redistribution in a rock only if any fluid–rock interaction at low temperatures can be ruled out.

9. CONCLUSIONS

The polymetamorphic rocks on Bårdsholmen island provide constraints both on the geologic evolution of the southern part of the Western Gneiss Region of Norway, and on contrasting mechanisms and processes of Sr isotope redistribution during metamorphism. From the combined petrological, geochemical, and isotopic data, the following conclusions can be drawn.

Granulite facies metamorphism occurred at 955 ± 3 Ma, at temperatures of 800–900 °C. The granulite facies rocks were later subducted, during the Caledonian orogeny, and partially eclogitized at 404 ± 2 Ma, with recorded P , T conditions of >650 °C at ~ 20 kbar. The eclogitization age is identical within error to available high-precision U–Pb zircon and Sm–Nd mineral isochron age data for the central part of the WGR, so that a contemporaneous and coherent subduction of the central and southern parts of the WGR appears likely. Eclogitization was incomplete and fluid-limited. Only in eclogite facies shear zones and along fluid pathways equilibrated eclogites were formed. Distal to fluid pathways, the granulites remained virtually ‘dry’ during metamorphism, and were largely metastably preserved. Eclogite facies overprint here only resulted in the diffusion-controlled growth of corona textures between granulite facies minerals. This setting is ideally suited to study the effects of solely thermally driven diffusion, independent from any recrystallization-inducing processes like deformation and fluid activity, on Sr isotope redistribution.

The minerals of the granulite facies assemblage have been exposed to temperatures exceeding 500 °C during the Caledonian orogeny for at least 5–10 Ma, with peak temperatures reaching 700 °C. Despite prolonged prevalence of high temperatures, intermineral Sr tracer diffusion did

not significantly alter Precambrian Sr signatures of feldspar, amphibole or pyroxene. It did not even fully reset biotite. Instead, closed system diffusive isotope transport has generated disequilibrium isotope distributions in the rocks, with a preferential but incomplete redistribution of Sr between the two least retentive phases, i.e., apatite and biotite. Based on our observations and literature data for comparable settings, we suggest that such a disequilibrium pattern, with isotope redistribution dictated by Sr diffusivities of the various minerals of an assemblage, is a characteristic signature for the impact of solely thermally driven diffusion. For practical purposes, overall intermineral disequilibria, combined with grain size vs. age correlations for mica and ‘excess’ radiogenic Sr in another high-diffusivity phase of a rock (like apatite) should be distinctive for a ‘diffusion pattern’.

The observation that prolonged thermal impact alone has been insufficient to re-equilibrate Sr isotopes among phases of polymineralic assemblages has some general consequences in geochronology.

First, it appears that diffusion may only be able to re-equilibrate Sr isotopes in thermally extreme situations, possibly during prolonged granulite facies metamorphism with subsequent rapid cooling. In other settings, diffusion will generally *not* lead to full intermineral Sr isotopic homogenization. Since initial isotopic homogeneity is a prerequisite for Rb–Sr isotopic dating, Rb–Sr mineral data cannot be interpreted in terms of ‘cooling ages’—a conclusion that can be drawn in analogy also for other isochron-based dating methods. This is just because if there is a multimineral isochron correlation (equivalent to a recorded event of full Sr-isotopic equilibration among *all minerals*) the equilibration was most likely not effected by temperature-driven diffusion, and if there is Sr-isotopic disequilibrium, the data cannot be interpreted in terms of ‘ages’.

Second, the finding that textural relics in a rock are likely to represent isotopic relics reminds to a principle known as ‘*What You See Is What You Get*’. This idea can be used to constrain *P–T*–time information beyond the pitfalls of closure temperature theories. As shown in this study, textural relics can be used to directly link petrological *P*, *T* data with age information. The granulite facies assemblage, a relic to both eclogite and subsequent amphibolite facies overprint, allows for derivation of Rb–Sr age data using low-diffusivity minerals, and for *P*, *T* determination of the dated granulite facies event. The eclogite facies assemblages in the fully equilibrated eclogites, which on the m scale again is a relic to amphibolite facies overprint, enable *P–T* determinations and yield concordant Rb–Sr multimineral isochrons, generating another *P–T*–time anchorpoint. In the sample set of this study, full Sr-isotopic intermineral equilibration in the eclogites during fluid- and deformation-aided eclogitization contrasts with stranded eclogitization and isotopic disequilibria in granulites only a few cm apart. This is clear evidence that in fact recrystallization, driven by deformation and/or fluid–rock interaction events, is the process dated by valid multimineral isochrons. This Rb–Sr-based conclusion may be generalized for other isochron methods of isotopic dating.

ACKNOWLEDGMENTS

We would like to thank A.K. Engvik (Univ. Oslo) for providing some samples, V. Kuntz, J. Herwig, and B. Stöcker (all GFZ Potsdam) for help with sample preparation and photographic work, H. Kemnitz (GFZ) and E. Wessel (FZ Jülich) for their efforts with CL imaging, and S. Sindern (RWTH Aachen) for some geochemical data. CL images were kindly provided by S. Galloway (GATAN, UK) and R. Ries (ZWL). Fieldwork was supported by GFZ Potsdam and Oslo University. Careful and constructive reviews by B. Bingen, K. Kullerud and M. Thöni are gratefully acknowledged.

REFERENCES

- Andersen T. B. (1998) Extensional tectonics in the Caledonides of southern Norway, an overview. *Tectonophysics* **285**, 333–351.
- Andersen T. B. and Jamtveit B. (1990) Uplift of deep crust during orogenic extensional collapse: a model based on field studies in the Sogn–Sunnfjord region of western Norway. *Tectonics* **9**, 1097–1111.
- Andersen T. B., Jamtveit B., Dewey J. F. and Swensson E. (1991) Subduction and exhumation of continental crust: major mechanisms during continent–continent collision and orogenic extensional collapse, a model based on the South Norwegian Caledonides. *Terra Nova* **3**, 303–310.
- Austrheim H. (1998) Influence of fluid and deformation on metamorphism of the deep crust and consequences for the geodynamics of collision zones. In *When Continents Collide: Geodynamics and Geochemistry of Ultrahigh-Pressure Rocks* (eds. B. R. Hacker and J. G. Liou). Kluwer, Dordrecht, pp. 297–323.
- Austrheim H. and Engvik A. K. (1997) Fluid transport, deformation and metamorphism at depth in a collision zone. In *Fluid Flow and Transport in Rocks: Mechanisms and Effects* (eds. B. Jamtveit and B. W. Yardley). Chapman and Hall, London, pp. 123–137.
- Baadsgaard H. and Van Breemen O. (1970) Thermally induced migration of Rb and Sr in an adamellite. *Eclogae Geol. Helv.* **63**, 31–44.
- Baxter E. F. and DePaolo D. J. (2002) Field measurement of high temperature bulk reaction rates II: interpretation of results from a field site near Simplon Pass, Switzerland. *Am. J. Sci.* **302**, 465–516.
- Berry H. N., Lux D. R., Andresen A. and Andersen T. B. (1994) Progressive exhumation during orogenic collapse as indicated by 40/39 Ar cooling ages from different structural levels, southwest Norway. *Geonyst* **22**, 20–21.
- Bingen B., Austrheim H., Whitehouse M. J. and Davis W. J. (2004) Trace element signature and U–Pb geochronology of eclogite-facies zircon, Bergen arcs, Caledonides of W Norway. *Contrib. Mineral. Petrol.* **147**, 671–683.
- Brabander D. J. and Giletti B. (1995) Strontium diffusion kinetics in amphiboles and significance to thermal history determinations. *Geochim. Cosmochim. Acta* **59**, 2223–2238.
- Brey G. P. and Köhler T. (1990) Geothermometry in four-phase lherzolites, II. New thermobarometers, and practical assessment of existing thermobarometers. *J. Petrol.* **31**, 1353–1378.
- Bryhni I. and Sturt B. A. (1985) Caledonides of southwestern Norway. In *The Caledonide Orogen—Scandinavia and Related Areas* (eds. D. E. Gee and B. A. Sturt). Wiley, pp. 89–107.
- Bryhni I. (1989) Status of the supracrustal rocks in the Western Gneiss Region, S. Norway. In *The Caledonian Geology of Scandinavia* (ed. R. A. Gayer). Graham and Trotman, London, pp. 221–228.

- Carswell D. A., Brueckner H. K., Cuthbert S. J., Mehta K. and O'Brien P. J. (2003a) The timing of stabilisation and the exhumation rate for ultra-high pressure rocks in the Western Gneiss Region of Norway. *J. Metamorph. Geol.* **21**, 601–612.
- Carswell D. A., Tucker R. D., O'Brien P. J. and Krogh T. E. (2003b) Coesite micro-inclusions and the U/Pb age of zircons from the Hareidland Eclogite in the Western Gneiss Region of Norway. *Lithos* **67**, 181–190.
- Chauvet A. and Dallmeyer R. D. (1992) $^{40}\text{Ar}/^{39}\text{Ar}$ mineral dates related to Devonian extension in the southwestern Scandinavian Caledonides. *Tectonophysics* **210**, 155–177.
- Cherniak D. J. and Ryerson F. J. (1993) A study of strontium diffusion in apatite using Rutherford backscattering spectroscopy and ion implantation. *Geochim. Cosmochim. Acta* **57**, 4653–4662.
- Cuthbert S. J., Carswell D. A., Krogh-Ravna E. J. and Wain A. (2000) Eclogites and eclogites in the Western Gneiss Region, Norwegian Caledonides. *Lithos* **52**, 165–195.
- Dahl P. S. (1997) A crystal-chemical basis for Pb retention and fission-track annealing systematics in U-bearing minerals, with implications for geochronology. *Earth Planet. Sci. Lett.* **150**, 277–290.
- Di Vincenzo G., Ghiribelli B., Giorgetti G. and Palmeri R. (2001) Evidence of a close link between petrology and isotope records: constraints from SEM, EMP, TEM and in situ ^{40}Ar – ^{39}Ar laser analyses on multiple generations of white micas (Lanternman Range, Antarctica). *Earth Planet. Sci. Lett.* **192**, 389–405.
- Dodson M. H. (1973) Closure temperature in cooling geochronological and petrological systems. *Contrib. Mineral. Petrol.* **40**, 259–274.
- Eiler J. M., Baumgartner L. P. and Valley J. W. (1992) Intercrystalline stable isotope diffusion: a fast grain boundary model. *Contrib. Mineral. Petrol.* **112**, 543–557.
- Ellis D. J. and Green D. H. (1979) An experimental study of the effect of Ca upon garnet–clinopyroxene Fe–Mg exchange equilibria. *Contrib. Mineral. Petrol.* **71**, 13–22.
- Engvik A. K., Austrheim H. and Andersen T. B. (2000) Structural, mineralogical and petrophysical effects on deep crustal rocks of fluid-limited polymetamorphism, Western Gneiss region, Norway. *J. Geol. Soc. Lond.* **157**(1), 121–134.
- Engvik A. K. and Andersen T. B. (2000) Evolution of Caledonian deformation fabrics under eclogite and amphibolite facies at Vårdalsneset, Western Gneiss Region, Norway. *J. Metamorph. Geol.* **18**, 241–251.
- Fortier S. M. and Giletti B. J. (1989) An empirical model for predicting diffusion coefficients in silicate minerals. *Science* **245**, 1481–1484.
- Foreman R., Andersen T. B. and Wheeler J. (2005) Eclogite-facies polyphase deformation of the Drosdal eclogite, Western Gneiss complex, Norway, and implications for exhumation. *Tectonophysics* **398**, 1–32.
- Fossen H. and Dallmeyer R. D. (1998) $^{40}\text{Ar}/^{39}\text{Ar}$ muscovite dates from the nappe region of southwestern Norway: dating extensional deformation in the Scandinavian Caledonides. *Tectonophysics* **285**, 119–133.
- Gaál G. and Gorbatshev R. (1987) An outline of the Precambrian evolution of the Baltic shield. *Precambrian Res.* **35**, 15–52.
- Giletti B. J. (1991) Rb and Sr diffusion in alkali feldspars, with implications for cooling histories of rocks. *Geochim. Cosmochim. Acta* **55**, 1331–1343.
- Giletti B. J. and Casserly J. E. D. (1994) Diffusion kinetics in plagioclase feldspars. *Geochim. Cosmochim. Acta* **58**, 3785–3793.
- Gilotti J. A. and Elvevold S. (1998) Partial eclogitization of the Ambolten gabbro-norite, north-east Greenland Caledonides. *Schweiz. Min. Petr. Mitt.* **78**, 272–293.
- Giorgis D., Cosca M. and Li S. (2000) Distribution and significance of extraneous argon in UHP eclogite (Sulu terrain, China): insight from in situ $^{40}\text{Ar}/^{39}\text{Ar}$ UV–laser ablation analysis. *Earth Planet. Sci. Lett.* **181**, 605–615.
- Glodny J., Bingen B., Austrheim H., Molina J. F. and Rusin A. (2002) Precise eclogitization ages deduced from Rb/Sr mineral systematics: the Maksyutov complex, Southern Urals, Russia. *Geochim. Cosmochim. Acta* **66**, 1221–1235.
- Glodny J., Austrheim H., Molina J. F., Rusin A. and Seward D. (2003) Rb/Sr record of fluid–rock interaction in eclogites: the Marun-Keu complex, Polar Urals, Russia. *Geochim. Cosmochim. Acta* **67**(22), 4353–4371.
- Glodny J., Ring U., Kühn A., Gleissner P. and Franz G. (2005) Crystallization and very rapid exhumation of the youngest Alpine eclogites (Tauern Window, Eastern Alps) from Rb/Sr mineral assemblage analysis. *Contrib. Mineral. Petrol.* **149**, 699–712.
- Griffin W. L. and Brueckner H. K. (1980) Caledonian Sm–Nd ages and a crustal origin for Norwegian eclogites. *Nature* **285**, 319–321.
- Hacker B. R., Andersen T. B., Root D. B., Mehl L., Mattinson J. M. and Wooden J. L. (2003) Exhumation of high-pressure rocks beneath the Solund Basin, Western Gneiss Region of Norway. *J. Metamorph. Geol.* **21**, 613–629.
- Hacker B. R. (2007) Ascent of the ultrahigh-pressure Western Gneiss Region, Norway. In *Convergent Margin Terranes and Associated Regions: A Tribute to W.G. Ernst* (eds. M. Cloos, W. D. Carlson, M. C. Gilbert, J. G. Liou and S. S. Sorensen). Geological Society of America Special Paper 419, pp. 171–184.
- Hoskin P. W. O. and Black L. P. (2000) Metamorphic zircon formation by solid-state recrystallization of protolith igneous zircon. *J. Metamorph. Geol.* **18**, 423–439.
- Jäger E. (1967) Die Bedeutung der Biotit Alterswerte. In *Rb–Sr Altersbestimmungen an Glimmern der Zentralalpen* (eds. E. Jäger, E. Niggli and E. Wenk). Beitr. Geol. Karte Schw., NF 66, pp. 28–31.
- Jenkin G. R. T. (1997) Do cooling paths derived from mica Rb–Sr data reflect true cooling paths? *Geology* **25**, 907–910.
- Jeong G. Y., Cheong C. S. and Kim J. (2006) Rb–Sr and K–Ar systems of biotite in surface environments regulated by weathering processes with implications for isotopic dating and hydrological cycles of Sr isotopes. *Geochim. Cosmochim. Acta* **70**, 4734–4749.
- Joesten R. (1991) Grain boundary diffusion kinetics in silicate and oxide minerals. In *Diffusion, Atomic ordering and Mass Transport: Selected Topics in Geochemistry* (ed. J. Ganguly). Advances in Physical Geochemistry 8, pp. 345–395.
- Krabbendam M. and Dewey J. F. (1998) Exhumation of UHP rocks by transtension in the Western Gneiss Region, Scandinavian Caledonides. In *Continental Transpressional and Transtensional Tectonics* (eds. R. E. Holdsworth, R. A. Strachan and J. F. Dewey). Geological Society, London, Special Publications 135, pp. 159–181.
- Krabbendam M., Wain A. and Andersen T. B. (2000) Pre-Caledonian granulite and gabbro enclaves in the Western Gneiss Region, Norway: indications of incomplete transition at high pressure. *Geol. Mag.* **137**, 235–255.
- Kretz R. (1983) Symbols for rock-forming minerals. *Am. Mineral.* **68**, 277–279.
- Krogh E. J. (1977) Evidence of Precambrian continent–continent collision in Western Norway. *Nature* **267**(5606), 17–19.
- Krogh E. (1988) The garnet–clinopyroxene Fe–Mg geothermometer—a reinterpretation of existing experimental data. *Contrib. Mineral. Petrol.* **99**, 44–48.
- Kühn A., Glodny J., Iden K. and Austrheim H. (2000) Retention of Precambrian Rb/Sr phlogopite ages through Caledonian

- eclogite facies metamorphism, Bergen Arc Complex, W-Norway. *Lithos* **51**, 305–330.
- Kullerød L. (1991) On the calculation of isochrons. *Chem. Geol.* **87**(2), 115–124.
- Kylander-Clark A. R. C., Hacker B. R., Johnson C. M., Beard B. L., Mahlen N. J. and Lapen T. J. (2007) Coupled Lu–Hf and Sm–Nd geochronology constrains prograde and exhumation histories of high- and ultrahigh-pressure eclogites from western Norway. *Chem. Geol.* **242**, 137–154.
- Labrousse L., Jolivet L., Andersen T. B., Agard P., Hébert R., Maluski H. and Schärer U. (2004) Pressure–temperature–time–deformation history of the exhumation of ultra-high pressure rocks in the Western Gneiss Region, Norway. In *Gneiss Domes in Orogeny*, pp. 155–183. Geological Society of America Special Paper 380.
- Leake B. E. and 20 others (1997) Nomenclature of amphiboles. Report of the subcommittee on amphiboles of the International Mineralogical Association Commission on new minerals and mineral names. *Eur. J. Mineral.* **9**, 623–651.
- Lovera O. M., Richter F. M. and Harrison T. M. (1989) The $^{40}\text{Ar}/^{39}\text{Ar}$ thermochronometry for slowly cooled samples having a distribution of diffusion domain sizes. *J. Geophys. Res.* **94**, 17917–17935.
- Ludwig K. R. (1980) Calculation of uncertainties of U–Pb isotope data. *Earth Planet. Sci. Lett.* **46**, 212–220.
- Ludwig K. R. (1993) Isoplot—a plotting and regression program for radiogenic isotope data. Version 2.70. *U.S. Geological Survey Open-File Report*, 91–445, pp. 1–42.
- Ludwig K. R. (1999) Isoplot/Ex Ver 2.06: a geochronological toolkit for Microsoft Excel. *Berkeley Geochronology Center Special Publications*, 1a.
- Montel J.-M., Kornprobst J. and Vielzeuf D. (2000) Preservation of old U–Th–Pb ages in shielded monazite: example from Beni Bousera Hercynian kinzigites (Morocco). *J. Metamorph. Geol.* **18**, 335–342.
- Mørk M. B. E. (1985) A gabbro to eclogite transition on Flemsøy, Sunnmøre, West Norway. *Chem. Geol.* **50**, 283–310.
- Norton M. G. (1987) The Nordfjord-Sogn Detachment. *Norsk Geologisk Tidsskrift* **67**, 93–106.
- Philippot P. and Selverstone J. (1991) Trace-element-rich brines in eclogitic veins: implications for fluid composition and transport during subduction. *Contrib. Mineral. Petrol.* **106**, 417–430.
- Pouchou J. L. and Pichoir F. (1985) “PAP” $\Phi(\rho z)$ correction procedure for improved quantitative microanalysis. In *Microbeam Analysis* (ed. J. T. Armstrong). San Francisco Press, pp. 104–106.
- Powell R. (1985) Regression diagnostics and robust regression in geothermometer/geo-barometer calibration: the garnet–clinopyroxene geothermometer revisited. *J. Metamorph. Geol.* **3**, 327–342.
- Ravna E. J. K. (2000) The garnet–clinopyroxene Fe^{2+} –Mg geothermometer: an updated calibration. *J. Metamorph. Geol.* **18**, 211–219.
- Ravna E. J. K. and Terry M. (2004) Geothermobarometry of UHP and HP eclogites and schists—an evaluation of equilibria among garnet–clinopyroxene–kyanite–phengite–coesite/quartz. *J. Metamorph. Geol.* **22**(6), 579–592.
- Røhr T. S., Corfu F., Austrheim H. and Andersen T. B. (2004) Sveconorwegian U–Pb zircon and monazite ages of granulite-facies rocks, Hisarøya, Gulen, Western Gneiss Region, Norway. *Norwegian J. Geol.* **84**, 251–256.
- Romer R. L. (1996) U–Pb systematics of stilbite-bearing low temperature mineral assemblages from the MalMBERGET iron ore, northern Sweden. *Geochim. Cosmochim. Acta* **60**, 1951–1961.
- Root D. B., Hacker B. R., Mattinson J. M. and Wooden J. L. (2004) Zircon geochronology and ca. 400 Ma exhumation of Norwegian ultrahigh-pressure rocks: an ion microprobe and chemical abrasion study. *Earth Planet. Sci. Lett.* **228**, 325–341.
- Schmid R., Wilke M., Oberhänsli R., Janssens K., Falkenberg G., Franz L. and Gaab A. (2003) Micro-XANES determination of ferric iron and its implication in thermobarometry. *Lithos* **70**, 381–392.
- Sengupta P., Dasgupta S., Bhattacharya P. K. and Mukherjee M. (1990) An orthopyroxene–biotite geothermometer and its application in crustal granulites and mantle-derived rocks. *J. Metamorph. Geol.* **8**, 191–197.
- Skår Ø. and Pedersen R. B. (2003) Relations between granitoid magmatism and migmatization: U–Pb geochronological evidence from the Western Gneiss complex, Norway. *J. Geol. Soc., Lond.* **160**, 935–946.
- Smith M. P. and Yardley B. W. D. (1999) Fluid evolution during metamorphism of the Otago schist, New Zealand: (II) Influence of detrital apatite on fluid salinity. *J. Metamorph. Geol.* **17**, 187–193.
- Sneeringer M., Hart S. R. and Shimizu N. (1984) Strontium and samarium diffusion in diopside. *Geochim. Cosmochim. Acta* **48**, 1589–1608.
- Stacey J. S. and Kramers J. D. (1975) Approximation of terrestrial lead isotope evolution by a two-stage model. *Earth Planet. Sci. Lett.* **26**, 207–221.
- Steiger R. H. and Jaeger E. (1977) Subcommittee on geochronology: convention on the use of decay constants in geo- and cosmochronology. *Earth Planet. Sci. Lett.* **36**, 359–362.
- Svensen H., Jamtveit B., Yardley B., Engvik A. K., Austrheim H. and Broman C. (1999) Lead and bromine enrichment in eclogite-facies fluids: extreme fractionation during lower-crystal hydration. *Geology* **27**, 467–470.
- Svensen H., Jamtveit B., Banks D. A. and Austrheim H. (2001) Halogen contents of eclogite facies fluid inclusions and minerals: Caledonides, western Norway. *J. Metamorph. Geol.* **19**, 165–178.
- Terry M. P., Robinson P. and Ravna E. J. K. (2000) Kyanite eclogite thermobarometry and evidence for thrusting of UHP over HP metamorphic rocks, Nordøyane, Western Gneiss Region, Norway. *Am. Mineral.* **85**, 1637–1650.
- Terry M. P. and Robinson P. (2003) Evolution of amphibolite-facies structural features and boundary conditions for deformation during exhumation of high- and ultrahigh-pressure rocks, Nordøyane, Western Gneiss Region, Norway. *Tectonics* **22**(4), 1036. doi:10.1029/2001TC001349.
- Tilton G. R., Ames L., Schertl H. P. and Schreyer W. (1997) Reconnaissance isotopic investigations on rocks of an undeformed granite contact within the coesite-bearing unit of the Dora Maira Massif. *Lithos* **41**, 25–36.
- Tucker R. D., Robinson P., Solli A., Gee D. G., Thorsnes T., Krogh T. E., Nordgulen & Oslash and Bickford M. E. (2004) Thrusting and extension in the Scandian Hinterland, Norway: new U–Pb ages and tectonostratigraphic evidence. *Am. J. Sci.* **304**, 477–532.
- Vance D., Müller W. and Villa I. M. (2003) Geochronology: linking the isotopic record with petrology and textures—an introduction. *Geol. Soc. Spec. Publ.* **220**, 1–24.
- Vavra G., Schmid R. and Gebauer D. (1999) Internal morphology, habit and U–Th–Pb microanalysis of amphibolite-to-granulite facies zircons: geochronology of the Ivrea Zone (Southern Alps). *Contrib. Mineral. Petrol.* **134**, 380–404.
- Villa I. M. (2006) From nanometer to megameter: isotopes, atomic-scale processes, and continent-scale tectonic models. *Lithos* **87**, 155–173.
- Wain A. L., Waters D. J. and Austrheim H. (2001) Metastability of granulites and processes of eclogitisation in the UHP region of Western Norway. *J. Metamorph. Geol.* **19**(5), 607–623.

- Walsh E. O. and Hacker B. R. (2004) The fate of subducted continental margins: Two-stage exhumation of the high-pressure to ultrahigh-pressure Western Gneiss Region, Norway. *J. Metamorph. Geol.* **22**, 671–687.
- Waters D. J. and Martin H. N. (1993) Geobarometry of phengite-bearing eclogites. *Terra Abstr.* **5**, 410–411.
- Wayte G. J., Worden R. H., Rubie D. C. and Droop G. T. R. (1989) A TEM study of disequilibrium plagioclase breakdown at high pressure: the role of infiltrating fluid. *Contrib. Mineral. Petrol.* **101**, 426–437.
- Wells P. R. A. (1977) Pyroxene thermometry in simple and complex systems. *Contrib. Mineral. Petrol.* **62**, 129–139.
- Wood B. J. and Banno S. (1973) Garnet–orthopyroxene and orthopyroxene–clinopyroxene relationships in simple and complex systems. *Contrib. Mineral. Petrol.* **42**, 109–124.

Associate editor: Yuri Amelin